AFOSR-TR- 80-1063

LEVEL II

(12)

AD A091300

AAE

AERONAUTICAL AND ASTRONAUTICAL ENGINEERING DEPARTMENT

ENGINEERING EXPERIMENT STATION, COLLEGE OF ENGINEERING, UNIVERSITY OF ILLINOIS, URBANA

80 10 21 022

LEVEL II

12

Aeronautical and Astronautical Engineering Department
University of Illinois at Urbana-Champaign

Technical Report AAE 80-1
UILU-Eng 80 0501

Prepared for

Air Force Office of Scientific Research
Aerospace Sciences Directorate
Bolling Air Force Base, D.C.

GAS FLOW RESISTANCE MEASUREMENTS THROUGH PACKED BEDS AT HIGH REYNOLDS NUMBERS

by

Stephen F. Wilcox and Herman Krier

Approved for public release; distribution unlimited
Grant No. AFOSR 77-3336 March 1980

(14) AAE-80-1, UILU-ENG-80-0501

UNCLASSIFIED

SECURITY CLASSIFICATION OF THIS PAGE (When Data Entered)

REPORT DOCUMENTATION PAGE		READ INSTRUCTIONS BEFORE COMPLETING FORM
1. REPORT NUMBER AFOSR-TR-80-1063	2. GOVT ACCESSION NO. AD-A091300	3. RECIPIENT'S CATALOG NUMBER
4. TITLE (and Subtitle) GAS FLOW RESISTANCE MEASUREMENTS THROUGH PACKED BEDS AT HIGH REYNOLDS NUMBERS		5. TYPE OF REPORT & PERIOD COVERED INTERIM TECHNICAL REPORT July 1978 – May 1980
		6. PERFORMING ORG. REPORT NUMBER Tech Report AAE 80-1
7. AUTHOR(s) Stephen F. Wilcox, Herman Krier		8. CONTRACT OR GRANT NUMBER(s) AFOSR-77-3336
9. PERFORMING ORGANIZATION NAME AND ADDRESS University of Illinois at Champaign-Urbana, Urbana, Illinois 61801		10. PROGRAM ELEMENT, PROJECT, TASK AREA & WORK UNIT NUMBERS 2308/A2 61102F
11. CONTROLLING OFFICE NAME AND ADDRESS Air Force Office of Scientific Research/NA, Building 410, Bolling Air Force Base, DC 20332		12. REPORT DATE March 1980
		13. NUMBER OF PAGES 73
14. MONITORING AGENCY NAME & ADDRESS (if different from Controlling Office) (12) 94		15. SECURITY CLASS. (of this report) UNCLASSIFIED
		15a. DECLASSIFICATION/DOWNGRADING SCHEDULE

16. DISTRIBUTION STATEMENT (of this Report)

Approved for public release; distribution unlimited

17. DISTRIBUTION STATEMENT (of the abstract entered in Block 20, if different from Report)

18. SUPPLEMENTARY NOTES

19. KEY WORDS (Continue on reverse side if necessary and identify by block number)

Gas Flow Resistance, Packed Beds
Coefficient of Drag for DDT Regime

20. ABSTRACT (Continue on reverse side if necessary and identify by block number)

This work reviews the literature on gaseous flow pressure resistance in packed beds and found important differences depending on test conditions and Reynolds number ranges. A test apparatus was constructed which allowed for the testing over a wide range of pressures, test conditions, and Reynolds number range several orders of magnitude higher than previously tested. From the resulting data it was ascertained that the classical Reynolds number dependency of the coefficient of drag is not correct for Reynolds numbers —

DD FORM 1473, 1 JAN 73 — EDITION OF 1 NOV 65 IS OBSOLETE

UNCLASSIFIED

SECURITY CLASSIFICATION OF THIS PAGE (When Data Entered)

176005

greater than 1000. A new correlation for the coefficient of drag was developed, which indicated that a new factor, the kinetic energy of the gases being forced through the bed, must be taken into account. This formula was shown to be valid for a Reynolds number range 1,000 - 100,000, for particles ranging in diameter from 1 mm through 6 mm. This correlation of transient two-phase flows at high pressures, as needed in the modeling effort for deflagration-to-detonation (DDT) in granular beds of propellant.

Accession For	
NTIS GRA&I	☒
DDC TAB	☐
Unannounced	☐
Justification	
By	
Distribution/	
Availability Codes	
Dist.	Avail and/or special
A	

Abstract

This work reviews the literature on gaseous flow pressure resistance in packed beds and found important differences depending on test conditions and Reynolds number ranges. A test apparatus was constructed which allowed for the testing over a wide range of pressures, test conditions, and Reynolds number range several orders of magnitude higher, than previously tested. From the resulting data it was ascertained that the classical Reynolds number dependency of the coefficient of drag is not correct for Reynolds numbers greater than 10^3. A new correlation for the coefficient of drag, given below, was developed, namely,

$$Fv = 3.33 \times 10^6 \cdot D_b \; Re/U_{avg}^2$$

This formula was shown to be valid for a Reynolds number range 10^3-10^5, for spherical particles ranging in diameter from 0.96mm through 6mm. This correlation is expected to provide better input for more accurate calculations of transient two-phase flows at high pressures.

Mention of the commercial products used in connection with the work reported here does not constitute an endorsement by the University of Illinois or the contracting agency.

TABLE OF CONTENTS

LIST OF SYMBOLS

Symbol	Description	Units
a	Constant	-
a'	Constant	-
A, A_{pipe}	Area of Test Section Chamber	ft^2
Ae	Exit Area of Nozzle	in^2
A^*	Throat Area of Nozzle	in^2
b	Constant	-
C_i	Constant i=1,6	-
D_b	Diameter of Bead	ft
D_c	Test Section Chamber Diameter	ft
D_{cyl}	Diameter of Cylindrical Particle	ft
f	Alternate Coefficient of Drag	(Eq. 7)
F_E	Ergun's Coefficient of Drag	(Eq. 6a)
F_{K-N}	Kuo/Nydegger Coefficient of Drag	(Eq. 11)
$\hat{F}_s$	Robbins/Gough Coefficient of Drag	(Eq. A-1)
F_y	General Coefficient of Drag	(Eq. 3a)
G	Mass Flow Rate (per unit area)	$\frac{lbm}{sec\text{-}ft^2}$
g	Acceleration Due to Gravity	ft/sec^2
g_c	Gravitational Unit Conversion Factor	$\frac{lbm\text{-}ft}{lbf\text{-}sec^2}$
L	Length over which Pressure Drop Measured	ft
M	Mach Number	-
$\dot{m}$	Mass Flow Rate	lbm/sec
N	Number of Beads	
P_a	Atmosphere Pressure	lbf/ft^2
P_e	Exit Pressure of Nozzle	lbf/ft^2
P_i, P_j	Pressure at Pressure Transducers, i and j	lbf/ft^2
P_o	Stagnation Pressure in Plenum Tank	lbf/ft^2

Symbol	Definition	Units
R	Gas Constant	$\frac{lbf\text{-}ft}{lbm\text{-}{}^{\circ}R}$
r_{bi}	Radius of Bead	ft
Re	Reynolds Number	(Eq. 4a)
T	Temperature	°R
T_o	Stagnation Temperature in Plenum Tank	°R
$T_{T.S.}$	Gas Temperature in Test Section	°R
U_{avg}	Average Gas Velocity in Packed Bed	ft/sec
U_g	Gas Velocity	ft/sec
U_p	Solid Particles Velocity	ft/sec
U_m	Superficial Velocity	ft/sec
α	Constant	-
γ	Specific Heat Ratio	-
Γ_1	Characteristic Time $\equiv \Delta x/U_{avg}$	sec
μ	Viscosity	$\frac{lbm}{sec\text{-}ft}$
ρ, ρ_m	Average Gas Density in Packed Bed	lbm/ft^3
ρ_g	Density of Gas	lbm/ft^3
ρ_b	Density of Bead	lbm/ft^3
ϕ	Porosity	-

CHAPTER 1

INTRODUCTION

The gaseous flow resistance through packed beds of various sized solid particles has been investigated by numerous researchers, both theoretically and experimentally. This work extends back to the days of Osborne Reynolds in the early 1900's. The factors which determine the energy loss (or pressure drop) are numerous, and the analysis require many simplifying assumptions. However, the four main factors that directly affect the resistance of gaseous flow through a packed bed are:

1. Rate of fluid flow
2. Viscosity and density of the fluid
3. Porosity and orientation of packing
4. Size, shape and surface roughness of particles

The first two factors pertain to the fluid and the last two the solids.

Fluid Properties

The pressure drop through a granular bed is proportional to the fluid velocity at low flow rates and approximately to the square of the velocity at higher flow rates. Reynolds was the first to derive a formula that related fluid resistance (pressure gradient) to motion, due to friction in the form:

$$\Delta P/L = au + b\rho u^2 \tag{1}$$

where ΔP is a pressure drop over a length L, ρ is the density of the fluid, u an average gas velocity, and a and b are constants. Dividing this equation by velocity yields:

$$\Delta P/Lu = a + b\rho u \tag{1a}$$

A plot of $(\Delta P/Lu)$ versus (ρu) produces a straight line. It was found that this expression accurately represented the relation between flow rate and pressure drop at very low Reynolds numbers. As the velocity approaches zero, it is seen that the ratio of pressure drop to velocity is a constant.

$$\lim_{u \to 0} \frac{\Delta P/L}{u} = a$$

According to Darcy's law, this contant is proportional to viscosity (μ). Taking the limit at high flow rates, the constant a is negligible compared to $b\rho u$, where ρu is the mass flow rate.

$$\lim_{u \to \infty} \frac{\Delta P/L}{u} = b\rho u \tag{1b}$$

This condition exists in turbulent flow where the flow resistance is due to kinetic energy losses. Hence, the above equation can be rewritten as

$$\Delta P/L = a'\mu u + b\rho u^2 \tag{1c}$$

where $a' = a/\mu$ (a factor pertaining to variables in solids only). The first term on the right hand side represents viscous energy losses and the last term, kinetic energy losses.

Solid Properties

Blake was the first (1914) to establish the dependency of pressure drop upon porosity, by using an analogy to a circular pipe. He developed two dimensionless groups:

$$\text{Group A} \equiv \frac{\Delta P}{\rho u^2} \cdot \frac{D_b}{L} \cdot \frac{\phi^3}{1-\phi} \quad ; \quad \text{Group B} \equiv \frac{D_b \ \rho u}{u(1-\phi)} \tag{1d}$$

Modified Friction Factor — Modified Reynolds Number

Here porosity, ϕ, represents volume fraction for the gases to penetrate

into the packed bed. See Figure 1a, for schematic of a packed bed and explanation of terms. Note that,

$$1 - \phi = \frac{\text{Volume Solids}}{\text{Volume Chamber}} = \frac{\frac{N \pi D_b^3}{6}}{\frac{\pi D_c^2}{4} L} \qquad (2)$$

where N = number of beads in the volume bounded by the cross sectional area ($\pi D_c^2/4$) and length L.

The calculated porosity is only an average porosity for the packed bed. Figure 1b, from Benenati and Brosilow, shows how the void fraction varies through a packed bed [2]. Since the sphere only makes point contact with the wall, the porosity approaches 1 at the wall and then oscillates until it dampens out at the average porosity of the packed bed, about 4 1/2 to 5 sphere diameters distance away from the test section wall.

Blake obtained a relation between Group A and Group B by plotting one against the other. His efforts failed because he did not realize the pressure drop was due to both kinetic and viscous energy losses simultaneously [1].

Later Burke and Plummer theorized that the total resistance was equal to the sum of individual particle resistance. They stated that viscous energy loss was proportional to $\frac{(1-\phi)}{\phi^2}$ and kinetic energy loss to $\frac{(1-\phi)}{\phi^3}$. However, they failed to realize the additive affects of these losses [1].

Kozeny arrived at viscous energy loss proportional to $\frac{(1-\phi)^2}{\phi^3}$, by assuming that the granular bed was equivalent to a group of similar parallel channels.

In 1949, Ergun and Orning furthered the work in this area and derived

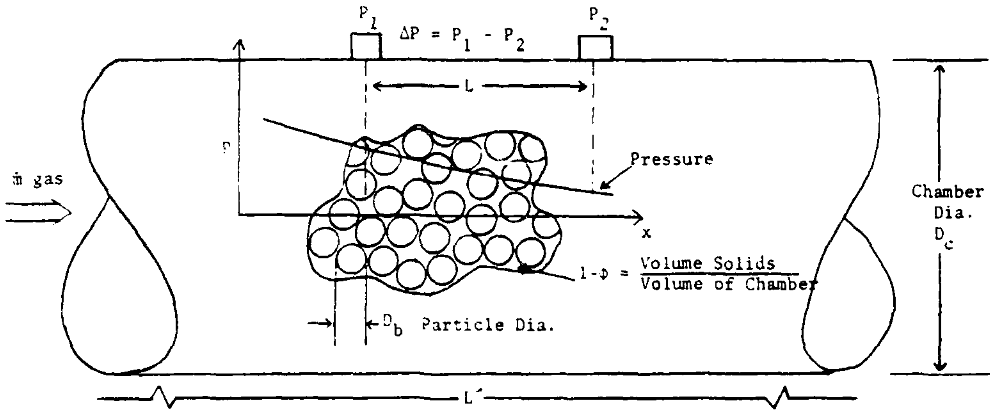

Figure 1a. Schematic of Packed Bed.

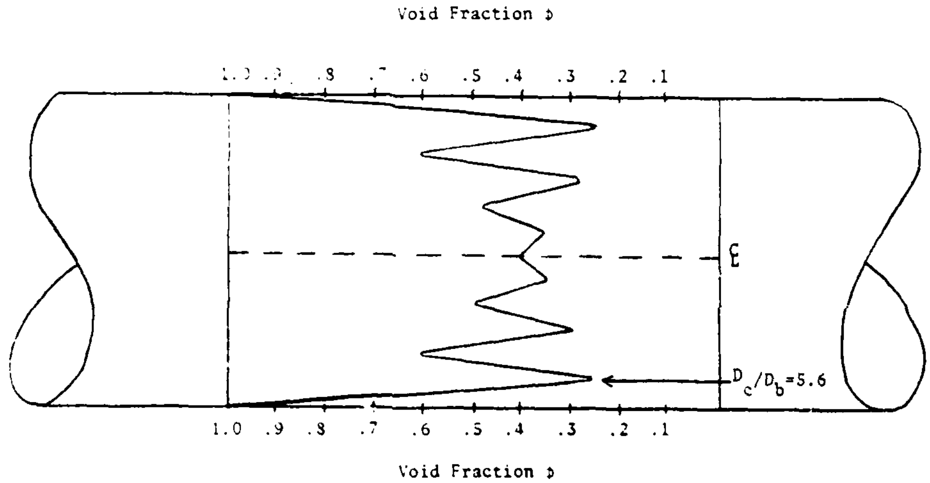

Figure 1b. Void Fraction in Beds of Uniform Spheres

an equation for drag per unit volume as follows [3]:

$$\frac{\Delta P}{L} = K_1 \cdot \frac{(1-\phi)^2}{\phi^3} \cdot \mu \frac{U_m}{D_b^2} + K_2 \cdot \frac{(1-\phi)}{\phi^3} \cdot \rho \frac{U_m^2}{D_b} \tag{3}$$

where $K_1 = 150$ and $K_2 = 1.75$, and U_m is the superficial velocity measured at an average pressure and based on the mass flow entering the packed bed. The coefficients K_1 and K_2 were determined by the method of least squares, from data representing 640 experiments using spheres, sand and pulverized coke with air and other gases including, CO_2, N_2, CH_4 and H_2 gases.

A transformation of equation (3) gives a more conventional (and non-dimensional) friction factor defined as,

$$F_v = \frac{\Delta P}{L} \cdot \frac{D_b^2}{\mu U_m} \cdot \frac{\phi^3}{(1-\phi)^2} \tag{3a}$$

where from equation (1)

$$F_v = 150 + 1.75 \frac{Re}{(1-\phi)} \tag{4}$$

and

$$Re = \rho \frac{U_m D_b}{\mu} \tag{4a}$$

Equation (4) gives a linear relationship between F_v and $\frac{Re}{(1-\phi)}$.

In 1951 Ergun further refined this formula, equation (3), by conducting experiments on a single system at various porosities [1]. His results included the superficial velocity, $U_m = \phi(U_g - U_p)$, which is due to the granular bed becoming mobile due to the high pressure, and velocity of the pressure front. It is based on empty column cross section. His resulting formula was,

$$\frac{\Delta P}{L} = 150 \frac{(1-\phi)^2}{\phi^2} \mu \frac{(U_g - U_p)}{D_b^2} + 1.75 \frac{(1-\phi)}{\phi^2} \rho \frac{(U_g - U_p)^2 \phi}{D_b} \tag{5}$$

which can be rearranged as:

$$\frac{\Delta p}{L} = \frac{\mu}{D_b^2}(U_g - U_p)\left\{\frac{(1-\phi)}{\phi^2}\left[150(1-\phi) + 1.75\,\frac{(U_g - U_p)}{\mu}\,\rho\phi D_b\right]\right\} \tag{5a}$$

or

$$\frac{\Delta p}{L} = \frac{\mu}{D_b^2}(U_g - U_p)\left\{\frac{(1-\phi)}{\phi^2}\left[150(1-\phi) + 1.75\text{ Re}\right]\right\} \tag{5b}$$

Equation (5b) can be used to define an alternate friction factor, i.e.,

$$\frac{\Delta p}{L} = \frac{\mu}{D_b^2}(U_g - U_p)\cdot F_E \tag{6}$$

where

$$F_E = \frac{(1-\phi)}{\phi^2}\left\{150(1-\phi) + 1.75\text{ Re}\right\} \tag{6a}$$

is the non-dimensional friction parameter. The subscript 'E', denotes the Ergun coefficient.

Equation (5) can be rearranged yielding a nondimensional <u>coefficient of drag</u>, f, in which

$$f \equiv \frac{\Delta p}{L}\,\frac{D_b\,\rho}{G^2}\,\frac{\phi^3}{(1-\phi)} \tag{7}$$

where $G = \rho\, U_{avg}\, \phi$

Comparing equation (7) with equations (6) and (6a), one sees that,

$$f = \frac{F_E\,\phi^2}{\text{Re}(1-\phi)} \tag{8}$$

Thus

$$f = \frac{\alpha}{\text{Re}} + b \tag{8a}$$

a correlation which is presented in Figure 2, taken from Bird, Stewart and Lightfoot [4]. Here α and b are constants equal to 150 and 1.75 respectifully. This figure graphically shows Ergun's work blending the limits of Blake-Kozeny equations and Burke-Plummer equations. The ordinate is equation (7) and the abscissa is Reynolds number defined in equation (4) divided by the solids loading $(1-\phi)$.

As stated above, Ergun's correlation was tested to a Reynolds numbers range of Re = 1380. This upper limit on the validity with respect to Reynolds number limits the application of this correlation. For example, the flow of gases in the ignition sequence in a ballistic system where the appropriate flow Reynolds number may reach 10^4 to 10^5. Recently Kuo and Nydegger obtained a different pressure loss expression for gas penetrating the tightly packed beds of small arms propellant grains, at a Reynolds number, about ten times as high as those used by Ergun [5]. They attempted to simulate the Reynolds number condition existing for the ignition sequence in a gun cartridge. Kuo and Nydegger used a cold flow test device with a 140 atmosphere compressor to provide the high pressure gas. They used actual propellant grains less than 1mm in diameter, so that they would obtain a true packing configuration. They tested at Reynolds numbers from 420 to 14,600 and their data provided the following correlation,

$$\frac{\Delta p}{L} = \frac{(1-\phi)^2}{\phi^3} \cdot \frac{\mu\phi(U_g - U_p)}{D_b^2} \cdot [5.05 \left(\frac{Re}{1-\phi}\right)^{0.87} + 276.23] \qquad (9)$$

This expression can be rewritten as

$$\frac{\Delta p}{L} = \frac{\mu}{D_b^2} (U_g - U_p) \cdot F_{K-N} \qquad (10)$$

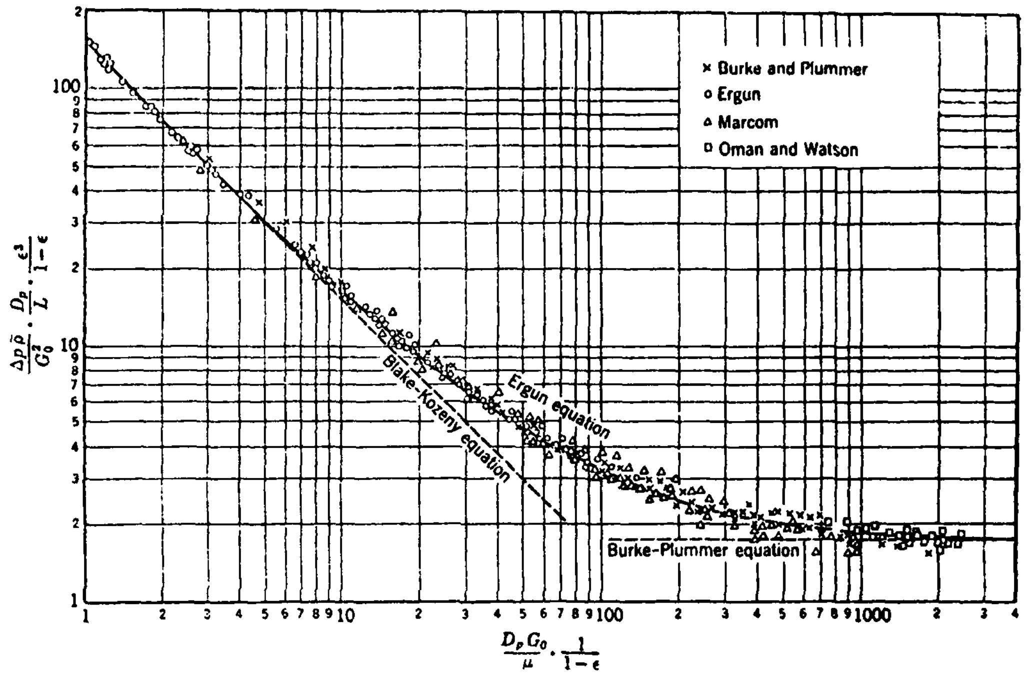

Figure 2. Sketch showing the general behavior of the Ergun Equation. [Figure taken from Ref. 4]

where the nondimensional friction factor, F_v for the Kuo/Nydegger tests, (called F_{K-N}) can be expressed as

$$F_{K-N} \equiv \frac{(1-\phi)^2}{\phi^2} \left[276.23 + 5.05 \left(\frac{Re}{1-\phi}\right)^{0.87}\right] \tag{11}$$

Figure 3 compares F_E and F_{K-N} as a function of a Reynolds number grouping $\frac{Re}{(1-\phi)}$. Note that Kuo arrives at a higher pressure drop than Ergun at low Reynolds number, and a lower drag than Ergun at high Reynolds number.

In 1978, Robbins and Gough developed an experimental apparatus to study the pressure drop through packed beds at Reynolds numbers appropriate to the flow sequence in large caliber cartridges [6]. They found that at Re $\sim 10^3$ their measured friction factor for spheres agreed reasonably well with Ergun's. However, at Reynolds number Re $\sim 10^5$, which is common to interior ballistics, their friction factor was 57% of Ergun's extrapolated results and 83% of Kuo's extrapolated values. They attempted to provide agreement of their data with the correlation of Kuo and Nydegger by utilizing an empirical correction factor based on the boundary layer developing from the chamber. It is not obvious that this logic is appropriate, since in fact the experiments of Kuo and Nydegger were carried out inside a very small diameter tube, while Robbins and Gough used a relatively large diameter test section. Based on Benenati and Brosilow [Reference 2] and Figure 1b, it seems logical that the boundary layer effect, as well as the best averaged uniform porosity occurs when D_c/D_b is large. For example D_c/D_b = 9.4 for Reference 5, while D_c/D_b ranged from 9.6 to 59.9 in the work reported in Reference 6.

Table 1 summarizes the work done by the above mentioned studies. Table 2 shows the relations between the drag force and the drag coefficient for each study. Note that Robbins and Gough do not actually

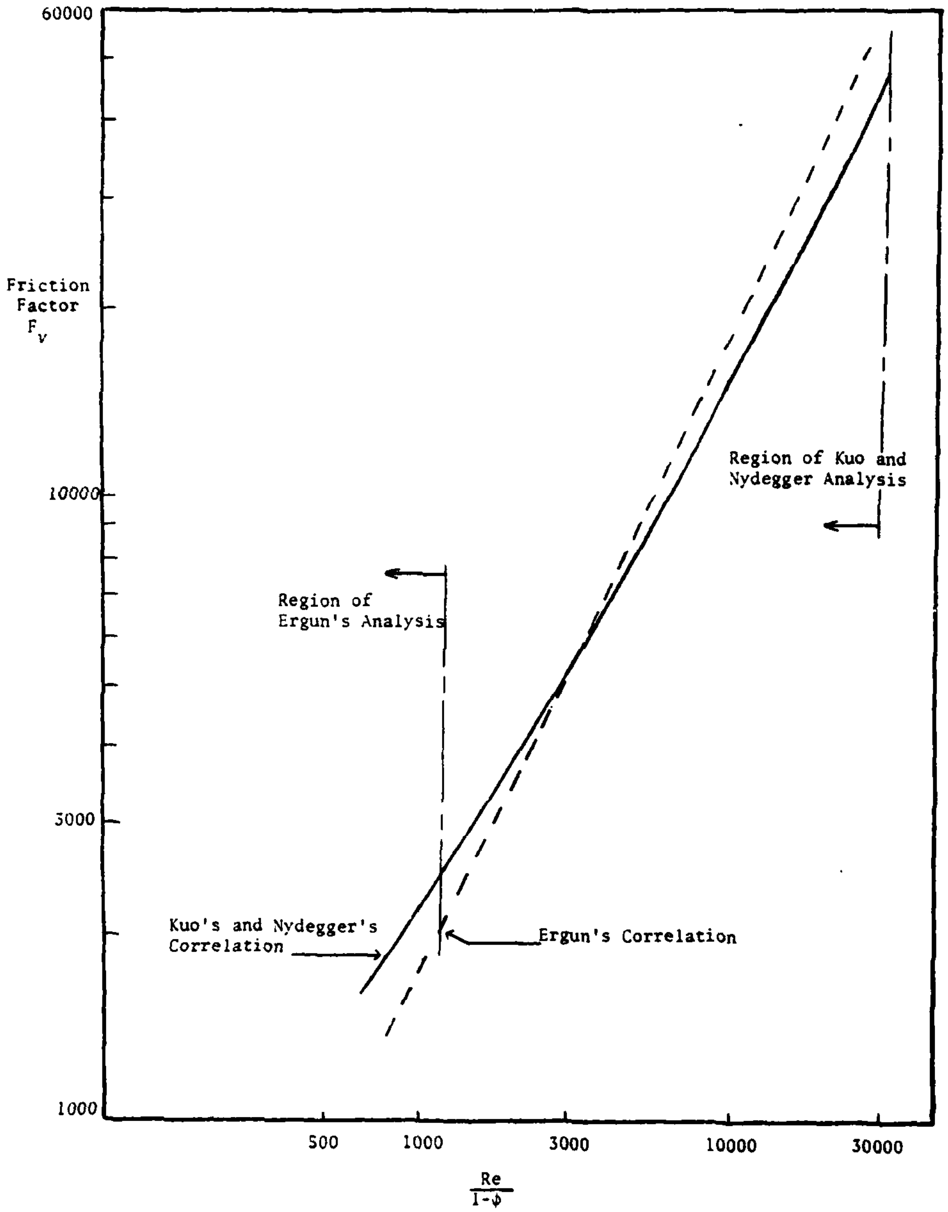

Figure 3. Ergun's Correlation Extrapolated to high Reynolds Numbers Compared to Kuo's and Nydegger's Correlation

Table 1. Summary of Drag Coefficient Studies

Experimenter	Reynolds #* Range	Porosity Range	Size Range	Max Pressure Source
Ergun (1952)	$0.35 \leq Re < 1380$	$0.40 < \phi < 0.65$	None Given	None Given
Kuo/Nydegger (1978)	$460 \leq Re \leq 14600$	$0.376 \leq \phi \leq 0.390$	0.826 mm (0.325 in.)	2038 psi**
Robbins/Gough (1978)	$778 \leq Re \leq 79200$	$0.389 \leq \phi \leq 0.396$	1.27 - 7.92 mm (0.05 - 0.3119 in.)	3000 psi**

$$*Re = \frac{\phi U_{avg} \rho_m D_b}{\mu}$$

** Actual gas pressures in the test bed were never reported.

Table 2. Drag Force Per Unit Volume and Drag Coefficient Relation

Investigator	F_v (Drag Coefficient)	Reynolds Number*
Ergun	$\frac{1-\phi}{\phi^2}\{150(1-\phi) + 1.75\ Re\}$	$0.35 \leq Re < 1380$
Kuo and Nydegger	$\frac{(1-\phi)^2}{\phi^2}\{276.23 + 5.05\ (\frac{Re}{1-\phi})^{0.87}\}$	$460 \leq Re \leq 14600$
Robbins and Gough (See Appendix A)	$\frac{(P_j^2 - P_i^2)\ \phi\ A^2\ D_b}{2\ \dot{m}^2\ RT\ L\ g_c} \cdot Re$	$778 \leq Re \leq 79200$

$$\frac{\text{Drag Force}}{\text{Unit Volume}} \quad \frac{\Delta P}{L} = \frac{\mu}{D_b^2}\ (U_g - U_p) \cdot F_v \qquad * Re = \frac{\phi U_{avg} \rho_m D_b}{\mu}$$

provide a correlation, but rather a method of utilizing measured pressure change values.

MOTIVATION

For the past three years work has been underway at the University of Illinois to analyze the unsteady reactive two-phase flow associated with DDT (Deflagration-to-Detonation-Transition) of confined granulated solid propellant and explosives. The theoretical models that have been developed, show there are constitutive relations which are "rate-determining" functions [7,8]. In addition, these relations are generally not well defined for unsteady flows at high pressure and high solids loading, the regime of most interest in the DDT problem. One of the most important of these constitutive relations is the gas-particle drag interaction. It basically determines the hot-gas permenability into the unignited portions of the granulated bed. This gaseous flow resistance has a profound effect on the flame spreading and combustion.

In order to investigate the gas-particle drag interaction, a cold flow experimental apparatus was developed by the author. In the future, it is planned to expand this test facility into a hot flow, dynamic pressure drop apparatus.

The drag measurements are initially made under steady-state conditions at high Reynolds numbers (10^4 - 10^5), and the results will be compared to work given in References 5 and 6. The test section was specified to be two inches in diameter compared to Robbins and Gough's 3 inch diameter section. The test section size was purposely different than those utilized by Ergun [1], Kuo and Nydegger [5], and Robbins and Gough [6], so that one could compare drag measurements for the same Reynolds

numbers to ascertain the wall confinement effects which have been briefly discussed above.

Since DDT is a transient phenomenon, it will also be desirable to compare the steady-state data with transient pressure data, to determine if the steady-state drag correlations given in Table 2 would in fact, be valid in a rapidly transient environment. The pressure level in the test section can be either increased with time as more gas is forced into the test section, or a high pressure gas tank can be emptied through the section providing a rapid decay.

Finally, if the data at the higher steady state Reynolds numbers or for the time-dependent Reynolds numbers, do not support the current correlations, then, if possible, a new correlation will be developed.

CHAPTER 2

EXPERIMENTAL APPARATUS

Introduction

This section details the design of the test apparatus and summarizes the test procedures. In designing the experimental apparatus, there were two major limiting factors, namely the pressure source currently available, and the funds available for fabrication and purchases of instrumentation.

The pressure source currently consists of a bank of nine compressed air tanks that supply a maximum working pressure of 450 psig, cold air flow. The packed-bed apparatus had to be designed around this limitation, yet be able to provide the required mass flow and Reynolds numbers of interest to this study.

Figure 4 gives a detailed schematic of the experimental apparatus from the plenum tank through the test section. The eight inch long test section, which contains the packed bed, is two inches in diameter. As stated previously, Kuo's and Nydegger's results were obtained from a 0.30 inch diameter test section, D_c, allowing the ratio $D_c/D_b = 9.4$. According to Benenatic and Brosilow [2], it seems that appropriate average porosity and minimum boundary layer effect occur with large D_c/D_b values, used for example by Robbins and Gough [6]. Hence, a test section diameter larger than Kuo's and Nydegger's [5], but smaller than Robbin's and Gough's was designed, since this would enable us to compare the drag measurements for identical conditions of particle size, mass flow and hence Reynolds number, but for different ratios of D_c/D_b.

The eight inch length of the test section was similar to other

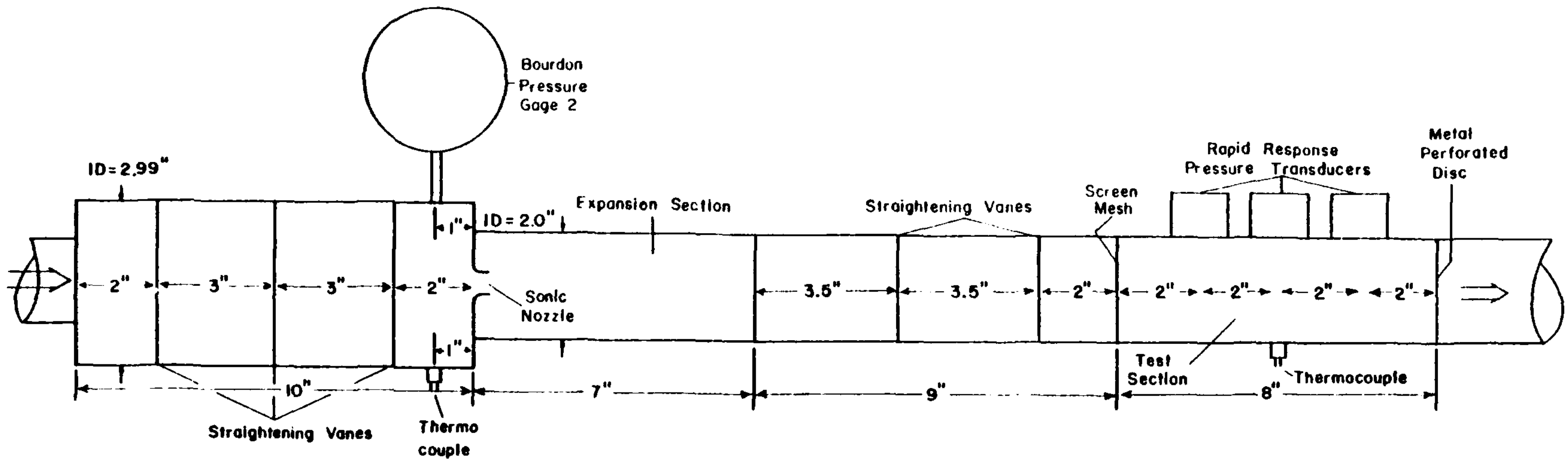

Figure 4. Detail Schematic of Plenum Tank through Test Section.

researchers, and allows enough distance from the ends of the test section to the first and last pressure transducer, so that the entrance and exit flow patterns do not bias the pressure data. Also the length chosen would diminish any errors that may occur due to nonuniformity in packing. The two inch distance between pressure transducers was arbitrarily chosen, but did allow for appropriate mounting of the gauges on the outside of the pipe test section. Three pressure transducers were chosen so that one could record at least two to three pressure gradients in the flow.

Details of Specific Hardware Utilized

Figure 5 is a schematic of the entire experimental apparatus. Bourdon gauge #1 is a Solfrunt 4.5 inch test gauge with a range of 0-1000 psig and a ± 0.25% of span accuracy. Its purpose is to continuously monitor the supply pressure. This is a moderately priced gauge, yet it has the range to be used with a higher pressure source. A Grove Pressure Reducing Regulator, Model 82-829 (720 psig max. inlet), allows us to regulate the compressed air source to the desired test pressure. This regulator could handle the source pressure, required mass flow, and in addition, regulate itself so that the desired test pressure in the plenum tank would not fluctuate. The 1-1/4 NPT pipe was compatable with the regulator and mass flow requirement.

The regulated compressed air enters a plenum tank with an inner diameter of 2.99 inches. This enlarged diameter, from 1.27 inch in the pipe, to 2.99 inch in the plenum, was designed to bring the gas to a very low velocity. The three straightening vanes are to smooth the flow of air in the plenum. Bourdon gauge #2 is the same type as Bourdon gauge #1. Gauge #2 indicates the test pressure, equal to the stagnation pressure P_o, which is used in the calculation of mass flow. At the end of the

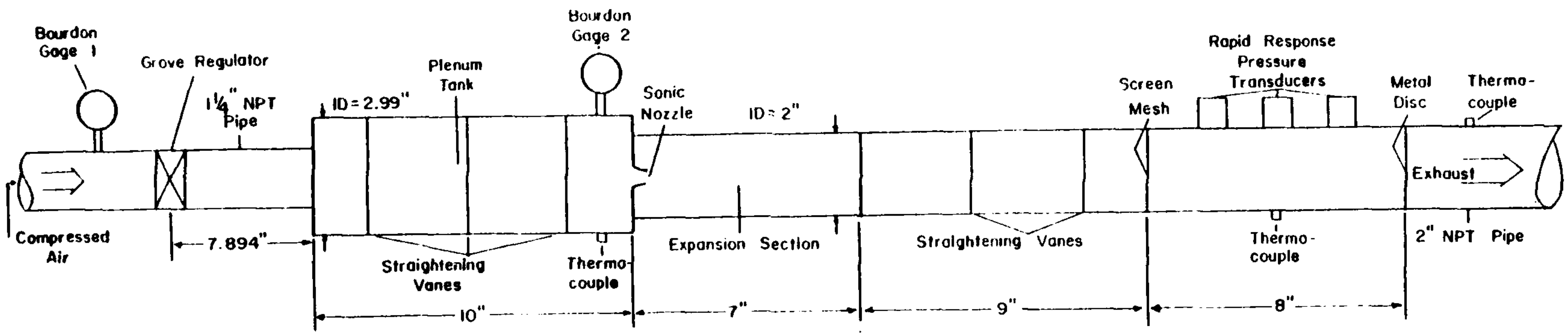

Figure 5. Entire Packed Bed Experimental Apparatus

plenum tank is a Sonic Flow Nozzle from the American Meter Division, Singer Corporation. This nozzle has a throat diameter of 0.375 inches, and an accuracy of ± 0.15% at 10 psig. This nozzle was selected because of its successful use by Robbins and Gough [6], its moderate cost, and its operation to provide the required mass flow rates. This nozzle, a converging-diverging nozzle, provided supersonic flow at its exit as explained in Appendix B. The high speed flow is then gently decelerated so that laminar flow enters the test section.

Opposite to the Bourdon gauge #2, is an Omega Thermocouple. It is a chromel-alumel, CASS-18G-12, grounded junction probe, that is designed to provide fast response under high pressures. This thermocouple measures the stagnation temperature, T_o (in the plenum tank) required for use in the mass flow calculation.

The sonic nozzle opens into an expansion section which connects into a straightening vane section. Based on the recommended minimum lengths of pipe preceding and following orifices, flow nozzles and venturies from the ASME "Fluid Meters," Chart [9], a nine inch long expansion-straightening section would be required. After running several tests in this configuration, it was decided to lengthen the expansion section, so that the flow would definitely be fully developed when it entered the test section.

All straightening vanes are, in fact, grids, constructed of 1/4 inch ground stock, so that the straightening vane is a mesh grid only 1/4 inch wide. Figure 6 is a photograph of one of the mesh grids as inserted into the straightening section. Note that several sets are positioned in the respective sections. The straightening vanes were constructed in this manner so that boundary layer interaction would be minimized.

The eight inch long and two inch diameter test section is directly

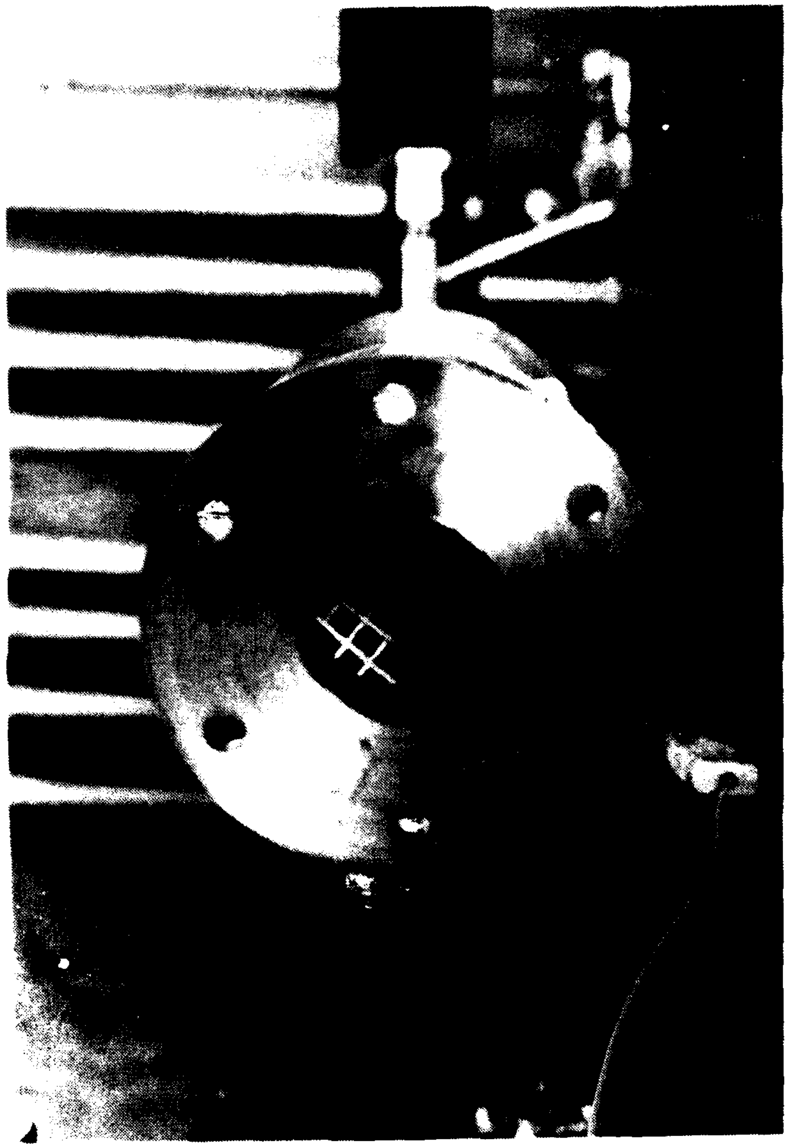

Figure 6. Straightening Vane Grid in Straightening Section.

mounted to the straightening section. This section has a screen mesh at the entrance and a metal stainless steel grid at the exit, to secure the packed bed in the test section as shown in Figure 7. There are three rapid response pressure transducers mounted on the test section to measure the pressure drop of the gas as it flows through the packed bed. The transducers are Setra Systems, Model 205, with a pressure range 0-500 psig, a one millisecond response time and an accuracy of 0.11% at full scale. This type transducer provides output signals for detection of any fluctuation in the steady-state air flow, and for continuous monitoring of the pressure in the transient tests.

The Omega thermocouples, as described previously, monitor the temperature in the test section and also after the gas exits the test section. All three thermocouples are connected to an Omega Digital Thermometer, Model 2160A, with a response time of less than 2 seconds, and a maximum error including NBS conformity of $\pm$ °1F. The Omega Thermocouples and digital thermometer were on hand and were used because they could accurately and rapidly record the temperatures.

For the decay transient experiments the regulator is not used. Instead a high pressure flex line (7000 psig limit) is connected one inch downstream from the regulator onto the pipe, as shown in Figure 8. This line is connected to a high pressure two way ball valve (3000 psig limit), which is connected to a compressed air bottle (2400 psig). Bourdon gauge #2 is replaced by a Setra System, Model 204E pressure transducer, (0-1000 psig), to continuously monitor the pressure in the plenum tank. The thermocouple in the plenum tank is connected to a storage oscilloscope, as described below. This allows the continuous monitoring of the temperature in the plenum tank, as the pressure decays or increases, whichever the

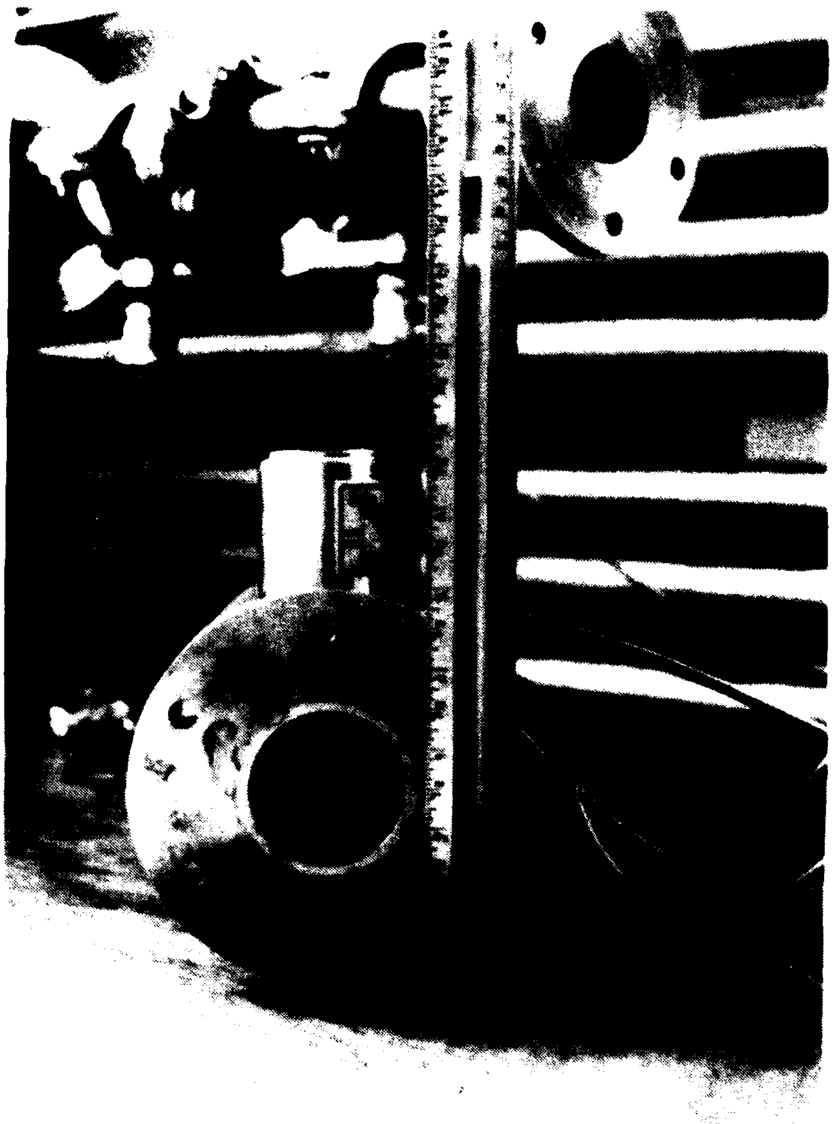

Figure 7. Packed Bed Retaining Grid.

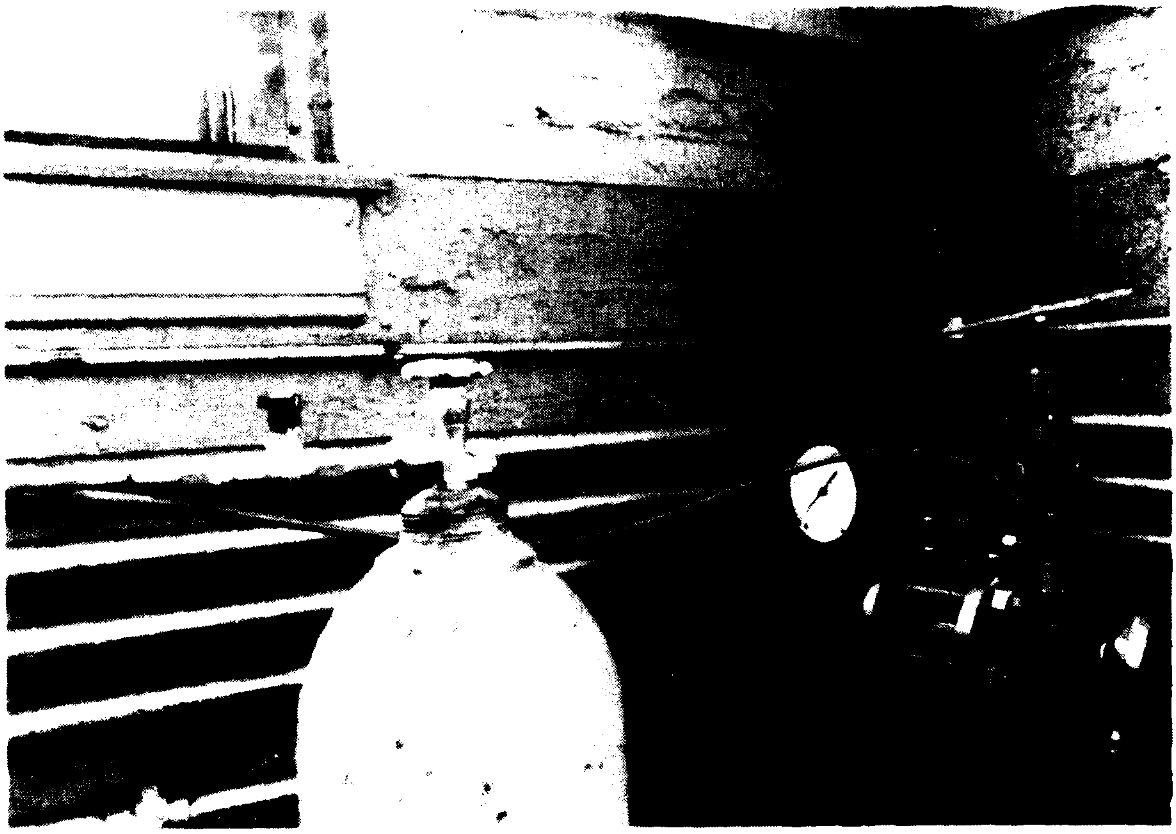

Figure 8. High Pressure Gas Bottle and Flex Line for Transient Experiment.

case may be. Figure 9 and 10 show the exterior of the apparatus ready for use in the steady state tests. Figure 11 shows the arrangement for the transient experiments.

The data from the Setra Transducers is recorded on a Tektronic 5100 series storage oscilloscope, and the traces are permanently recorded with a Tektronix C-5 oscilloscope camera. Thermo Systems, Model 1076, digital RMS voltmeters, were also used as a back up and comparison check when recording the steady state output from the transducers.

The wall thickness of the various pipes and tubing were determined by performing a hoop stress analysis of each individual section, so that each section could withstand a maximum pressure of 1000 psi with a safety factor of five.

Reduced Chamber Diameter

In order to determine the effect on the measured pressure gradient of the wall boundary layer build up and possible channeling of flow through the "annular" region at the wall, a sleeve was designed to be inserted into the test section. The metal sleeve was press fit into the section, such that the pressure port holes were aligned with the original pipe section. The insert was one inch in diameter, reducing the flow area of the standard two inch diameter test section by one fourth. This was done so that measurements could be carried out at two different ratios of D_c/D_b, for the same size beads. Discussions were given in the previous chapter which indicate why this type of data may be required. Table 3 summarizes the components for the packed bed test facilities used by Kuo and Nydegger [5], Robbins and Gough [6], and this study.

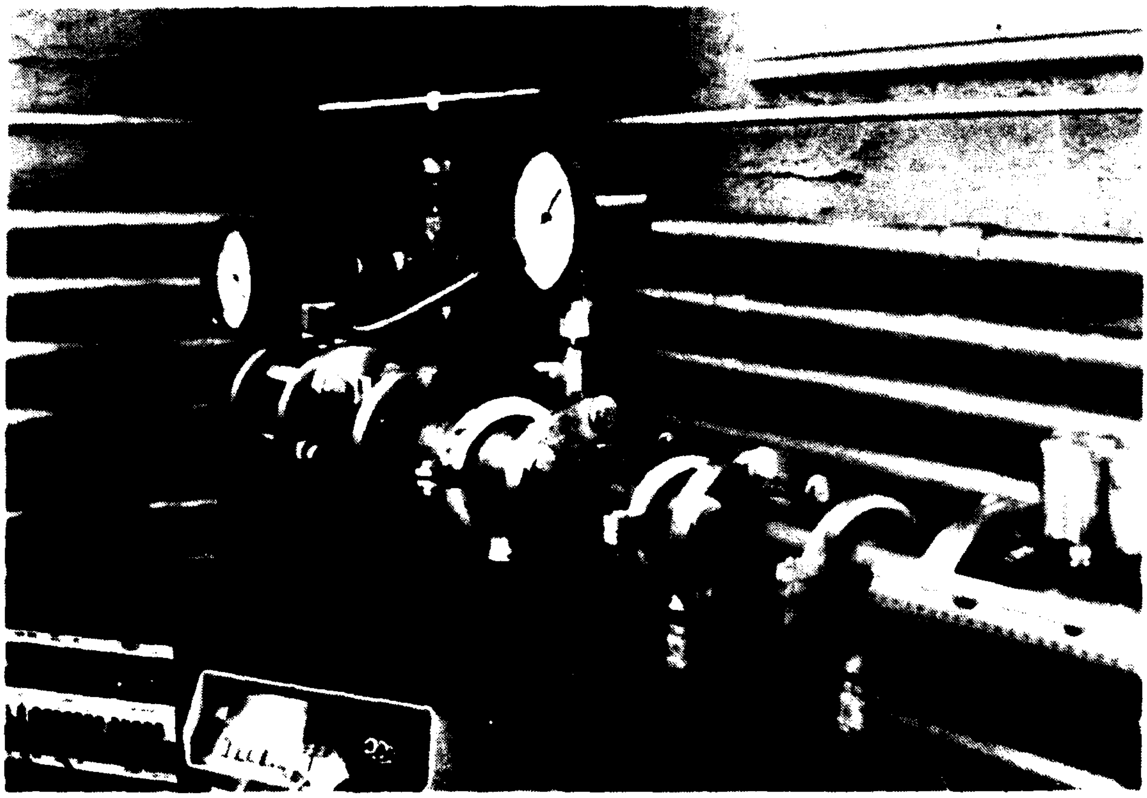

Figure 9. Exterior of Test Apparatus for Steady State Tests.

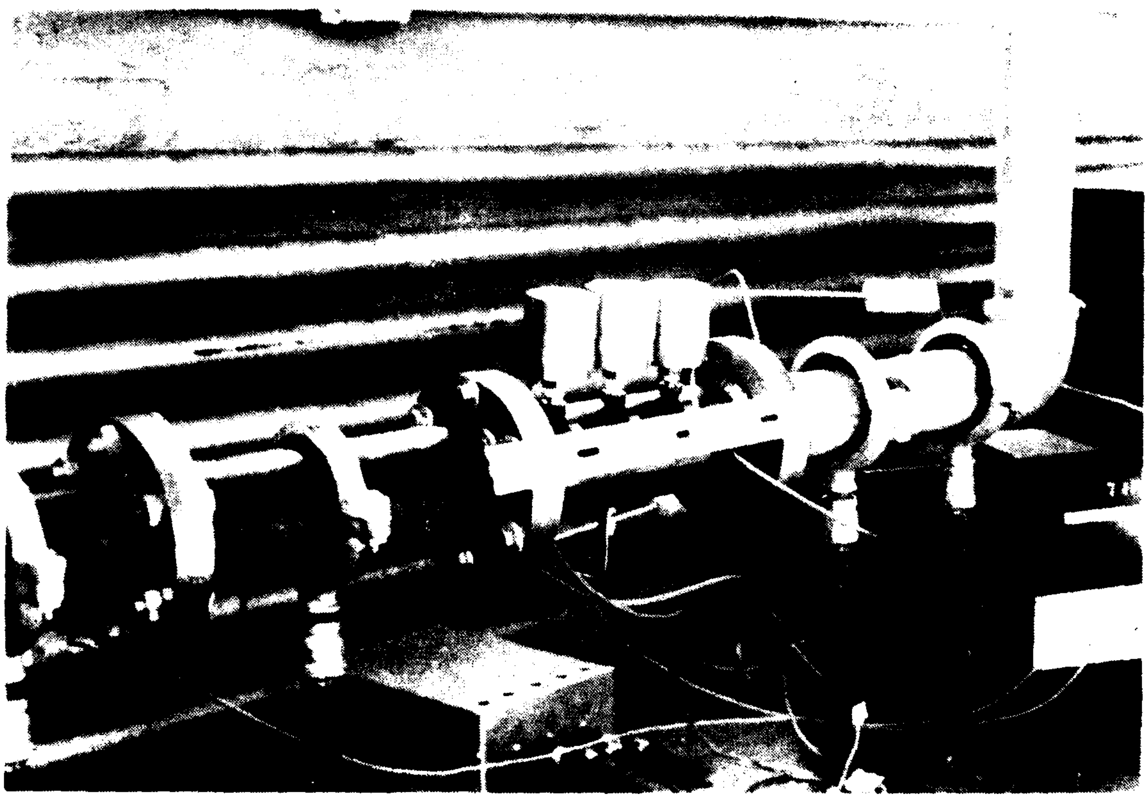

Figure 10. Exterior of Test Apparatus for Steady State Tests.

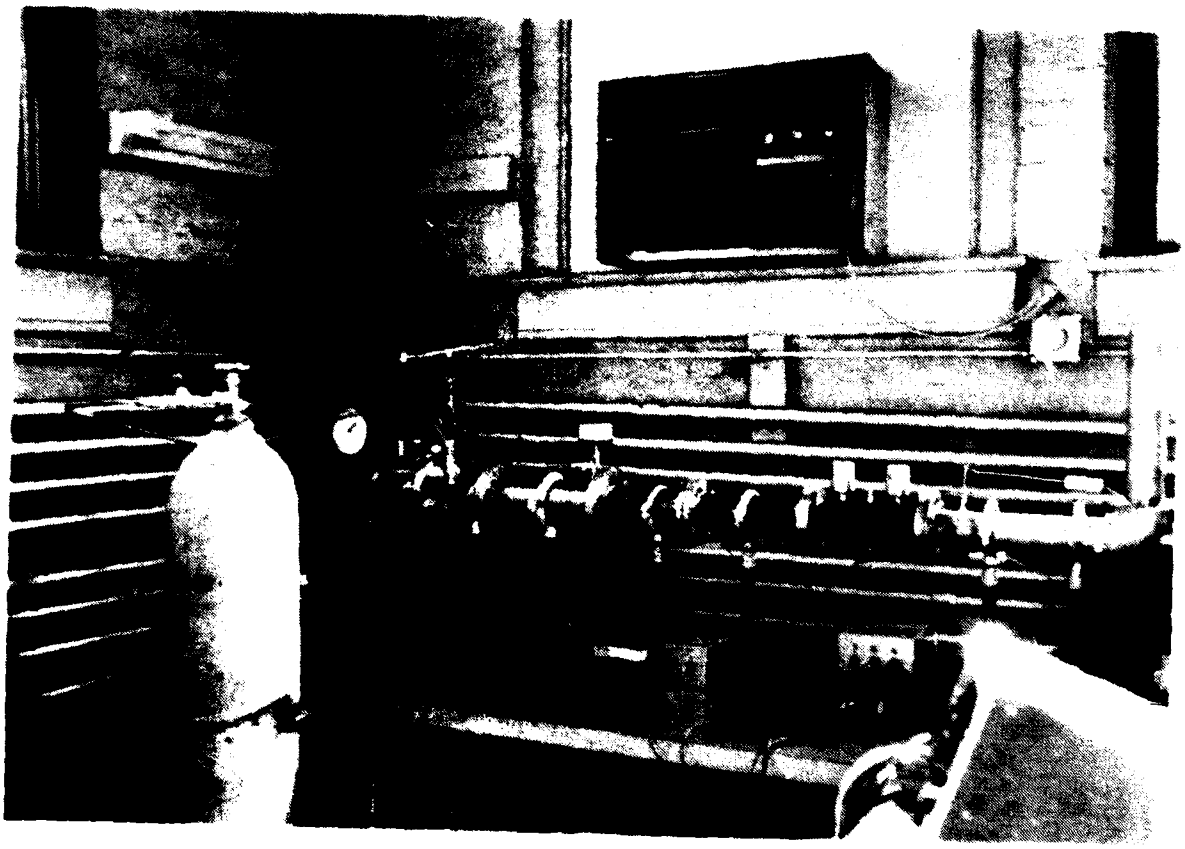

Figure 11. Experimental Apparatus in Transient Configuration.

Table 3. Comparison of Test Facilities

	Kuo/Nydegger	Robbins/Gough	Wilcox/Krier
Test Chamber Diameter D_c	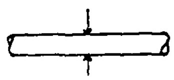 0.3059 in. (.777 cm)	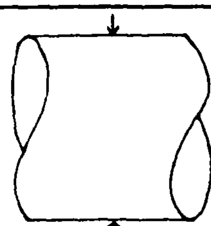 3 in. (7.62 cm)	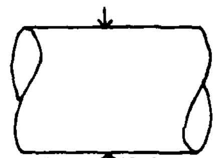 2 in. (5.08 cm) **
Diameter of Beads Tested D_B	0.826 mm(.0325 in.)	1.27 mm(.05 in.) 4.75 mm(.1870 in.) 7.922 mm(.3119 in.)	.96 mm(.0379 in.) 3 mm(.1204 in.) 6 mm(.2381 in.)
Test Chamber diameter to Bead diameter Ratio D_c/D_b	$\frac{D_c}{D_b} = 9.4$	$9.6 \leq \frac{D_c}{D_b} \leq 59.9$	$8.5 \leq \frac{D_c}{D_b} \leq 52.6$
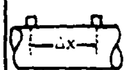 Distance between Pressure Transducers, Δx. Distance over which Pressure Drop Measured, ΔL.	Δx = 4 in. (10.16 cm) ΔL = 8 in. (20.32 cm)	Δx = 7.5 in. (19.05 cm) ΔL = 22.5 in. (57.15 cm)	Δx = 2 in. (5.08 cm) ΔL = 4 in. (10.16 cm)
Peak Pressure In Test Chamber (+Estimated)	187.0 psia (+)	544.0 psia (+)	360 psia

** Test section insert can reduce D_c to 1.0 inch .

Calibration and Experimental Procedure

The Bourdon gauges and pressure transducers were all calibrated on a dead weight tester prior to being installed on the experimental apparatus. These calibrations compared favorably with those supplied by the gauge manufacturer. See Appendix C for calibration details.

The experimental procedures for conducting steady state and transient experiments can be found in Appendix D. The most important factor when conducting the experiments was to compact the test bed at a higher pressure than would be used during the tests. This ensures that the packed bed will not further compact during the tests.

The experimental data obtainable from this apparatus is limited by the compressed air source of 450 psig, unless high pressure air bottles are manifolded into the plenum. In the latter case the time for carrying out steady-state (high-pressure) experiments is limited as these tanks empty.

The input pressures available limit the flow rate and consequently the Reynolds number range that presently can be studied. It is not now possible to obtain heated, high pressure air with this apparatus.

Specific Experiments Performed

Flow resistance experiments were performed mainly using the two inch diameter test section in which spherical beads of 0.96, 3.0, and 6.0 mm diameter were packed. The pressure gradient data was reduced, analyzed, and compared to the theoretical correlation of Ergun, Kuo and Nydegger, as well as to the experimental data of Robbins and Gough.

Table 4 summarizes almost all of the steady-state experiments performed. The combination mixture of 6 mm and 0.96 mm beads was made to determine any correlation between pressure drop, porosity and size mixing.

Table 4. Steady-State Experiments

(a) Two Inch I.D. Test Section

Particle Size	Particle Density (gr/cm^3)	Average Porosity (ϕ)	Steady State Pressures Tested (psig)	Range of Reynolds Number
Sphere D_b = 6 mm (.2381 in.)	2.57	0.402	25, 50, 100, 150, 200, 250, 300, 350, 400	$7470 \leq Re \leq 77{,}188$
Sphere D_b = 3 mm (.1204 in.)	2.58	0.387	(same as above)	$3784 \leq Re \leq 38{,}991$
Sphere D_b=0.96mm (.0379 in.)	2.98	0.394	(same as above)	$1207 \leq Re \leq 12{,}445$
Combination 6mm/0.96mm 50 % each by weight	N/A	0.296	100, 150, 200, 250, 300, 350, 400	$4534 \leq Re \leq 16{,}189$
Cylinders L=0.403 in. D_{cyl}=.183 in	4.78	0.443	100, 150, 200, 250, 300, 350, 400	$16595 \leq Re \leq 59251$

Table 4. Steady-State Experiments

(b) One Inch I.D. Test Section

Particle Size	Particle Density (gr/cm^3)	Average Porosity (ϕ)	Steady State Pressure Tested (psig)	Range of Reynolds Number
Sphere D_b = 6mm (0.2381 in.)	2.57	0.4394	50, 100 150, 200 250, 300 350, 400	$49175.3 \leq Re \leq 311861.3$
Sphere D_b = 3mm (0.1204 in.)	2.58	0.4068	(Same as above)	$24851.4 \leq Re \leq 157705.4$
Sphere D_b = 0.96mm (0.0379 in.)	2.98	0.4086	(Same as above)	$7784.2 \leq Re \leq 49605.2$

(Obviously, many more mixture ratios, small/large, could be tested.)

The packed bed of inert cylindrical propellant was tested at the same pressures used for the spherical beads. The pressure drop data was used to verify the observations made by Robbins and Gough [6] about the geometrical scaling of particles on the bed resistance.

The following chapter summarizes the data and the conclusions that can be drawn from these steady-state experiments.

Transient Pressure Input

There are two type transients, progressive and decay. The progressive transient occurs when the pressure in the test section is increased from 0 psig to 400 psig very rapidly, by opening the regulator. The decay transient occurs when a high pressure air bottle, which is attached to the apparatus as previously explained, is allowed to empty from 2400 psig to the room atmospheric pressure.

The time for the progressive transient depends only on how rapidly one is able to completely open the regulator by hand. Presently, it takes from one to two seconds.

The time for the decay transient depends on two factors. First, the total volume of the air in the bottle will dictate how long it takes to flow through an opening. Typical commercially available bottles of high pressure air, are tanks with volumes of 309 ft^3 or 296 ft^3. Secondly, the size of the opening in the air bottle will determine how much air can pass out of the bottle per second. In our specific case the manufacturer of the air bottle has specified the size of the opening from the bottle, and this can not be changed.

In Appendix E, the method for calculating the time to empty a pressure chamber is explained. It takes 2.73 minutes (164 seconds) for our

decay transient, using an air bottle with 309 ft^3 of air at an initial pressure of 2400 psig and at room temperature.

The transient pressure output at each of the three pressure transducers in the test section were recorded on an oscilloscope. This continuous pressure gradient data for the 0.96 mm, 3 mm and 6 mm diameter beads was compared to the discrete steady-state data, to determine whether the drag in the steady-state case was the same as that in the transient case.

CHAPTER 3

ANALYSIS OF TEST RESULTS

Attempt to Correlate Data with Known Formula

As was discussed in the first chapter, from measurements of a pressure gradient through a packed bed one can define a coefficient of drag F_v, by

$$F_v = \frac{\Delta P}{\Delta L} \frac{D_b^2}{\mu U_{avg} g_c} \tag{12}$$

For the test conditions as outlined in Table 4 (Chapter 2) this coefficient was calculated utilizing the above relation, where U_{avg} is determined by the mass flow. (Refer to Appendix B.) Table 2 lists two specific formulas for the drag coefficient as reported in the literature by Ergun [3] and Kuo and Nydegger [5].

Figure 12 plots these correlations as a function of Reynolds number as lines of constant porosity, ϕ. It should be noted that the correlation by Ergun has been extrapolated well beyond the range of Reynolds number where this correlation was developed. For the two inch interior diameter test section, the calculated F_v [from equation (12)] is plotted for three initial size spherical beads. The porosities for each test grouping is noted on the graph.

It would appear that for the larger particles (3mm and 6mm), the correlation by Kuo and Nydegger is adequate. Unfortunately, the sub-millimeter beads, provided data that gives Fv significantly less than that correlation, at least in the range of Reynolds number tested here. This is surprising since the work reported in Reference 5 utilizes sub-millimeter diameter beads, (0.826mm). As was shown in Table 3 of the previous chapter,

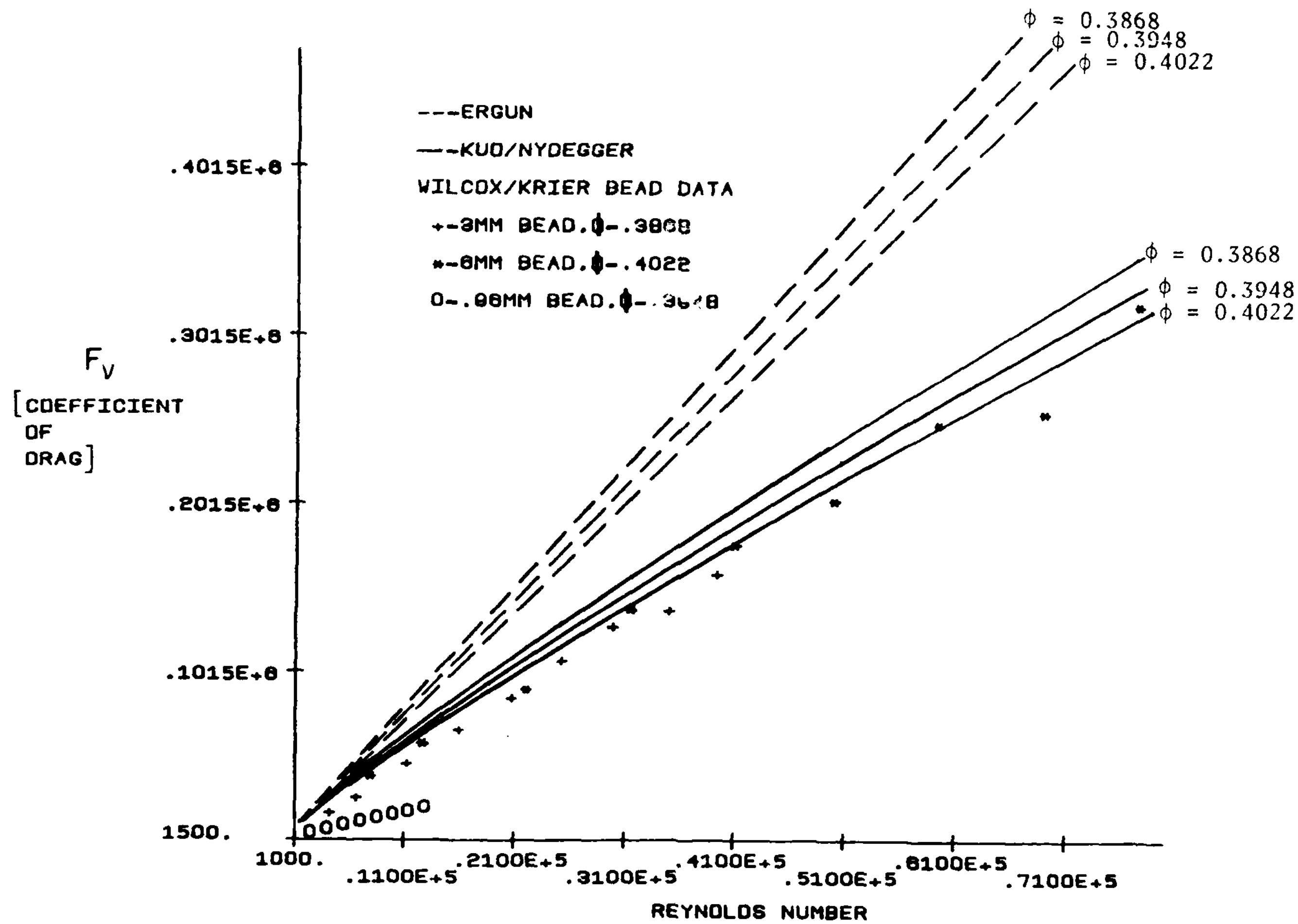

Figure 12. Comparison of Current work with Ergun's and Kuo/Nydegger Correlations.

the ratio of test chamber diameter to bead diameter, D_c/D_b, for the Kuo and Nydegger experiments was a value less than ten. For the 0.96mm spherical beads used here, this ratio was greater than fifty. It should be noted that when using the 6mm diameter beads, the ratio D_c/D_b is eight and a half, a number approaching that used in Ref. 5. Note that this condition correlates well with the published formula for F_v.

In order to more clearly determine the effect of the containers, i.e., the test section diameter, a smaller test section, exactly one inch interior diameter was utilized. Table 4b has summarized the tests performed with that modified apparatus. Since the area of this section is now one fourth that of the two inch test section, one achieves much higher average velocities for the same mass flows. Therefore, the range of the test Reynolds number is greatly extended. The Reynolds number range now available was well above those in the tests in Reference 5. Figure 13 presents the coefficient of drag, F_v, versus Reynolds number for the smaller diameter test section. The data clearly indicates that the correlation proposed by Kuo and Nydegger is no longer valid for this flow regime. It now appears that there are no particles within the range tested, that would fit the correlation of Reference 5, as there were, when the larger diameter test section was utilized.

Robbins and Gough [6] had also reported that their pressure drop data could only be marginally described by the correlation of Kuo and Nydegger. Their data also indicates, as was done here, that the correlation of Ergun should not be used at these large values of Reynolds numbers. Some of the data reported by Robbins and Gough will be compared with our findings in a following section.

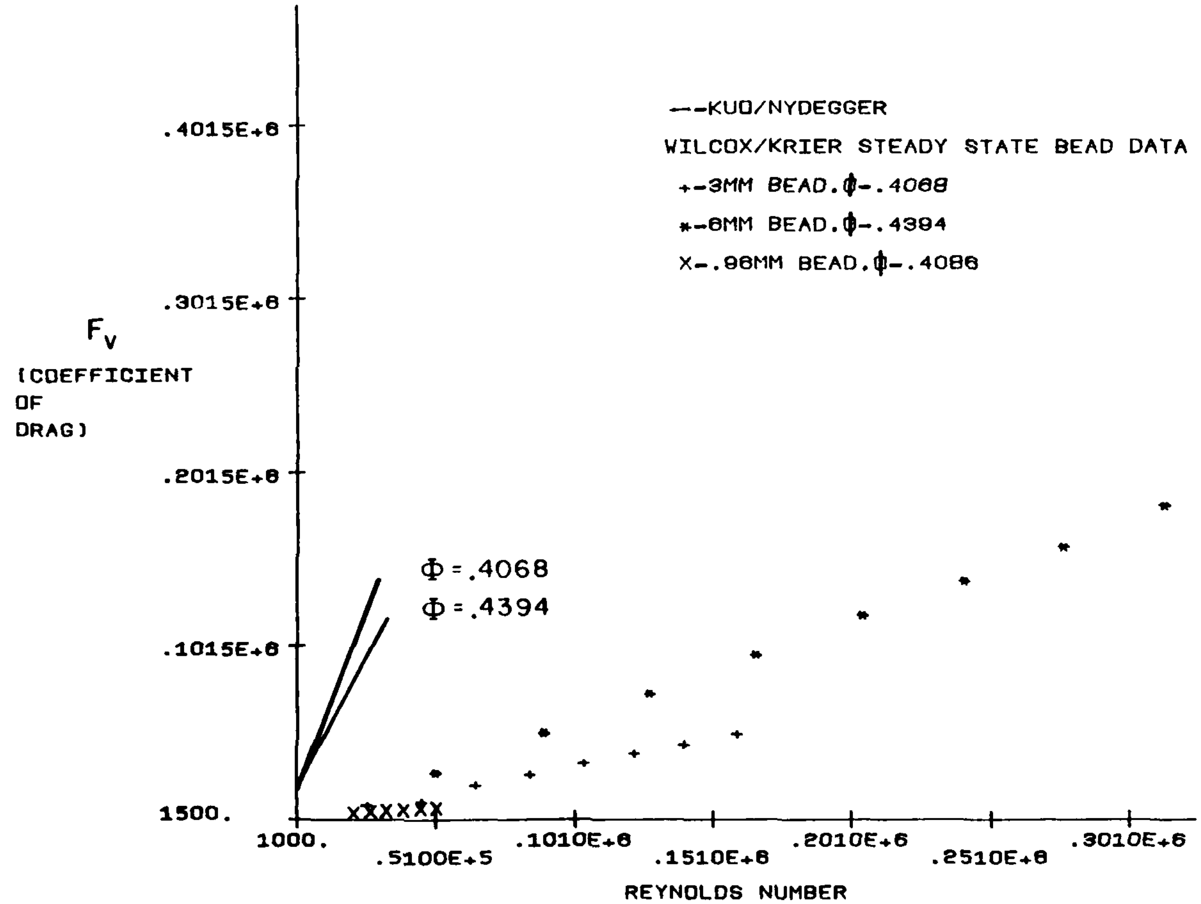

Figure 13. Comparison of 1 inch Test Section Data with Kuo/Nydegger Correlation [5].

Search for High Reynolds Number Drag Coefficient

When reviewing the type of data shown in the previous two figures, it becomes evident that one does not arrive at one unique coefficient of drag at a fixed Reynolds number when the test sections provide for a different flow area. That is, for any one fixed size spherical bead, a plot of F_v versus Reynolds number gives a relation that has a significantly different slope. Data shown on Figure 14 for the 0.96mm bead [Part (a)] and the 3mm bead [Part (b)], clearly bear this out.

The variation shown in Figure 14 is due to the fact, that at the same Reynolds number, the average velocity is significantly different. Equal Reynolds number at different average velocities is achieved by adjusting the average gas density (or pressure). Since $Re = \dot{m}\, D_b/A_{pipe}\, \mu$, this is achieved by altering the mass flow to match the change in pipe area. One must conclude that F_v is not solely a function of the flow Reynolds number as has been summarized by previous investigators and as reviewed in Chapter 1.

After inspection of the pressure drop data, it was found that for any given size bead, irrespective of the test section flow area, F_v correlates as a function of Re/U_{avg}^2. This is shown in Figure 15, indicating that the data given in Figure 14 collapses to one line when F_v is plotted as a function of Re/U_{avg}^2. This correlation is only approximately true for the tests with the 6mm spheres, but this is probably due to the fact that for the one inch interior diameter test section, the 6mm beads are too large to represent a uniformly packed bed.

Further replotting of the data showed that the effect of the bead size can also be correlated if one plots F_v as a function of $bD_b\, Re/U_{avg}^2$, where b = a constant. That correlation is shown in Figure 16. Here the

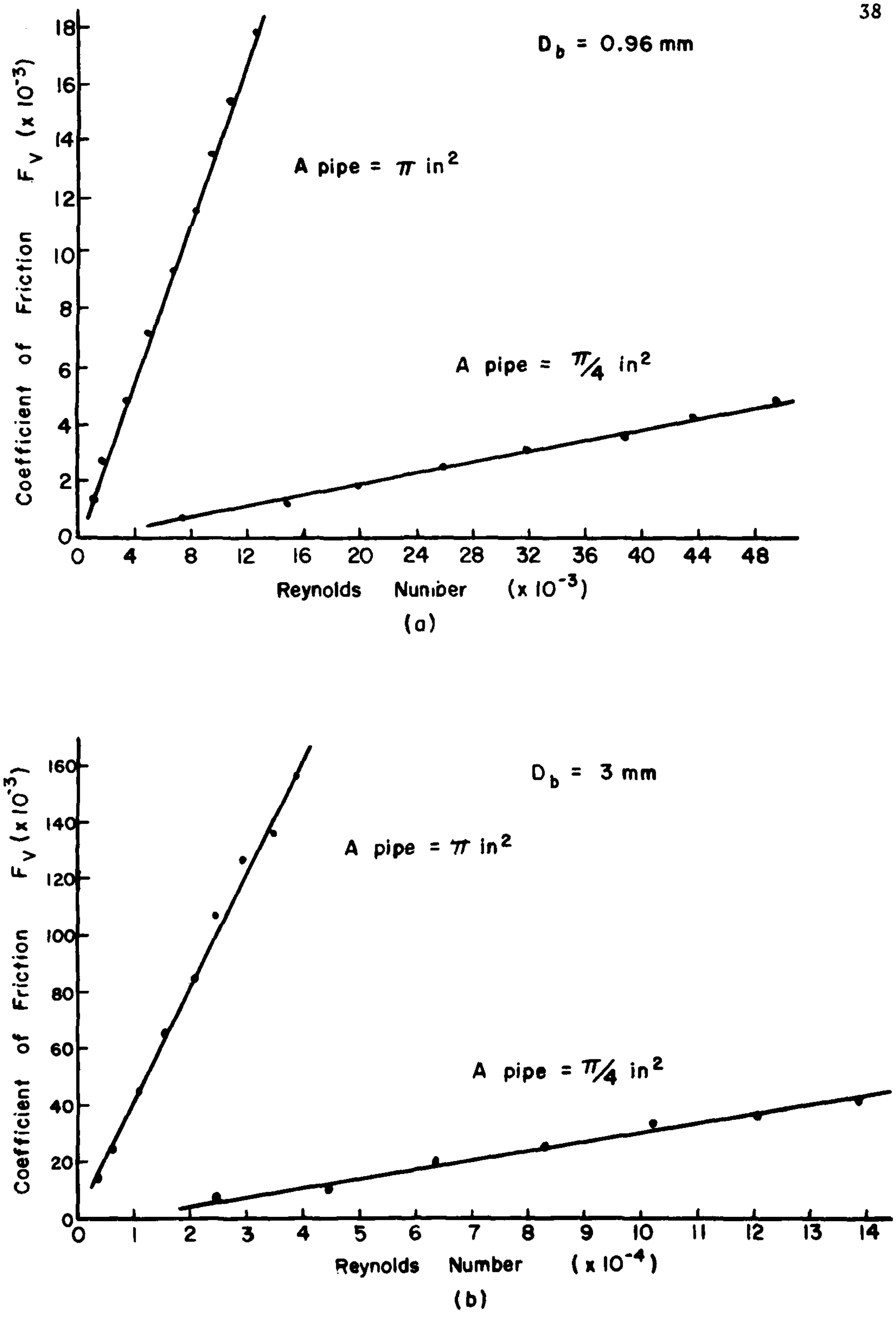

Figure 14. Variation in Coefficient of Drag for 2 inch and 1 inch Test Sections.

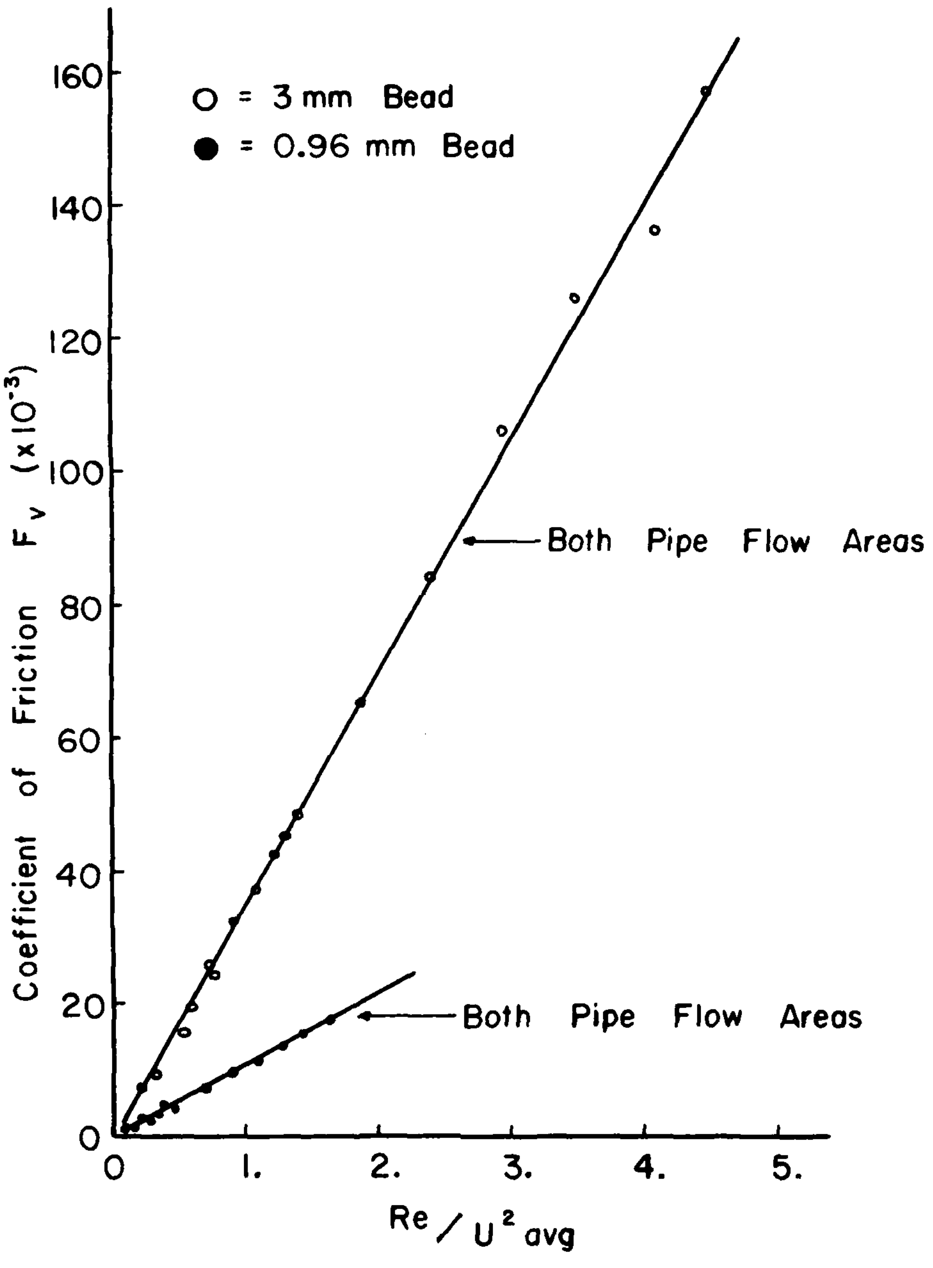

Figure 15. Coefficient of Drag as a Function of Reynolds Number and Velocity.

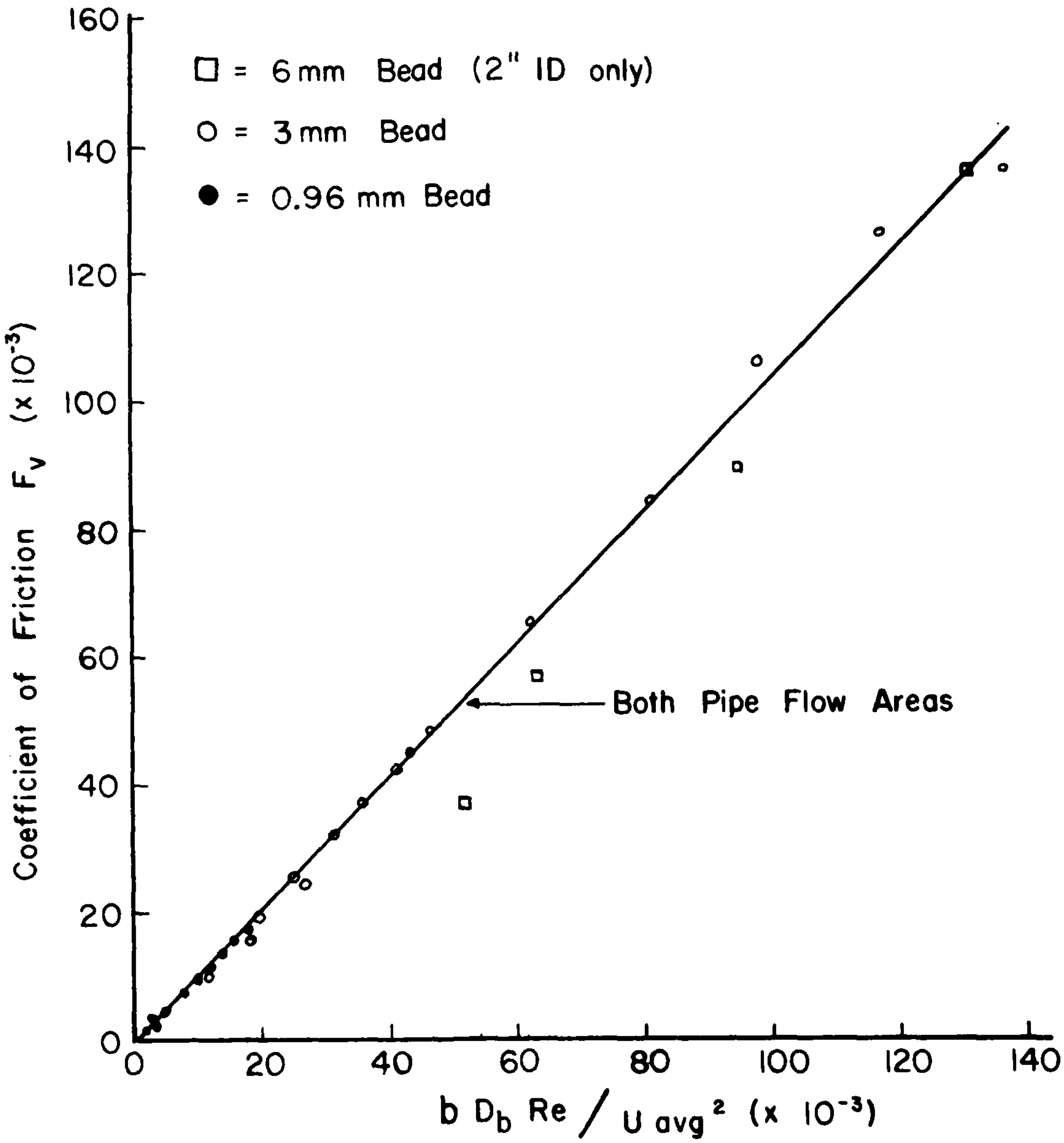

Figure 16. Coefficient of Drag as a Function of Bead Size, Reynolds Number and Velocity.

6mm bead data (with the 2 in. I.D. test section) also correlates with this functional relation.

This surprising correlation of coefficient of drag with the flow parameter indicates that the flow velocity, or more correctly, the kinetic energy of the flow ($\sim U_{avg}^2$) is a rate determining factor for F_v. Figure 17 plots F_v versus Reynolds number only. The data shown here is identical to that given in Figure 14b, except that the data of Robbins and Gough for a sphere nearest the 3mm bead tested here, is added. As has been indicated in Table 3 (Chapter 2), Robbins and Gough carried out their experiments in a three inch interior diameter pipe. Table 5 below summarizes the range of average velocities tested with the sections used here and with the apparatus used by Robbins and Gough, and Kuo and Nydegger.

Table 5. Average Flow Velocities

Investigator	Test Section Diameter (inch)	Range of U_{avg} (Fps)
Wilcox/Krier	1.00	305 - 340
Wilcox/Krier	2.00	83 - 132
Robbins/Gough	3.00	54 - 98ǂ
Kuo/Nydegger	0.3059	23 - 121ǂ

ǂ Estimated

It appears that for moderately low velocities (below 100 fps), a unique correlation between F_v and Reynolds number is possible. But for the higher average gas velocity, a correlation of the nature indicated in Figure 16 is more likely.

An alternate way to show that Reynolds number alone does not correlate the resistance to flow in a packed bed, is to plot an alternate

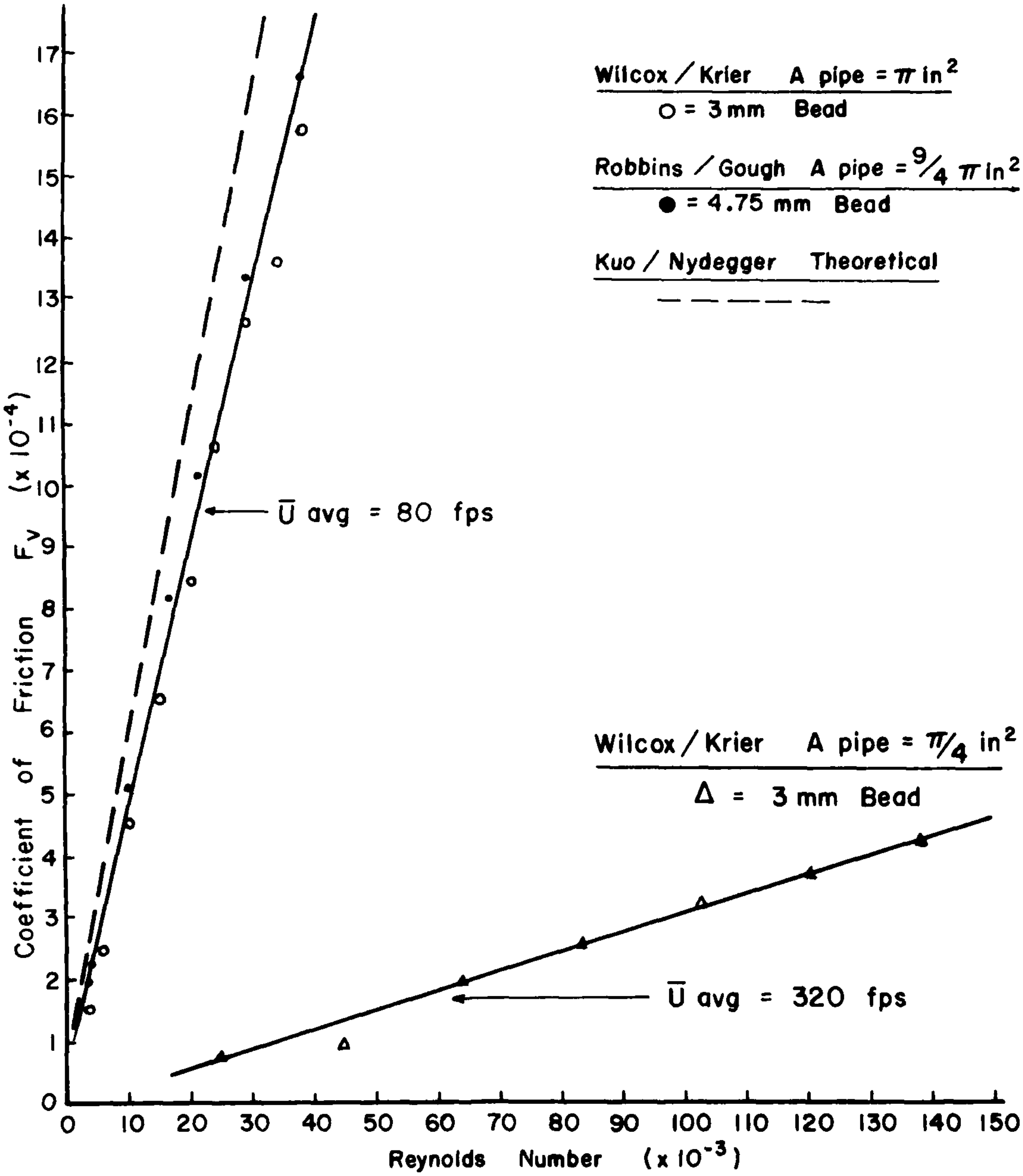

Figure 17. Comparison of Drag Coefficient Data, Indicating Flow Velocity Effect.

coefficient of drag, f, as defined in Eqs. (7) and (8). The data presented by Robbins and Gough is represented in this form. Clearly a velocity effect other than that given in the Reynolds number, dominates this altered form of the coefficient of drag, as shown in Figure 18, where f is plotted versus Reynolds number.

Formulation of High Reynolds Number Drag Coefficient

The classical equation for the coefficient of drag is $F_v = a + b\,Re$, based on Ergun's work [1], or more specifically Eq. (4), $F_v = 150 + 1.75 \cdot Re/(1-\phi)$. As discussed, the data at the higher Reynolds numbers indicate that this type of linear relation with Reynolds number is not correct. Instead, one notes that for the current study,

$$F_v = b \frac{Re}{U_{avg}^2} \tag{13}$$

Upon comparing Eq. (13) with the data, it was found that b was a function of bead diameter. A plot of b versus D_b on log-log paper resulted in a fairly accurate condition that

$$b = a\,D_b \tag{14}$$

where $a = 3.33 \times 10^6$ ft/sec^2. Equation (13) then becomes

$$\boxed{F_v = (3.33 \times 10^6 \text{ ft/sec}^2)\, D_b \frac{Re}{U_{avg}^2}} \tag{15}$$ ǂ

where F_v is nondimensional, as required. Recall that Eq. (4a) defines the Reynolds number, and Eq. (B-3) the average gas velocity, U_{avg}, as

$$Re = \rho \frac{U_{avg}\,\phi\,D_b}{\mu} \qquad U_{avg} = \frac{\dot{m}}{\rho\,\phi\,A_{pipe}}$$

Substituting Eq. (15) into Eq. (12), the pressure gradient becomes,

ǂ This correlation was specifically developed at moderate to high gas velocities, and for Reynolds number greater than 10^3. It should not be extrapolated to very low velocities, since $F_v \to \infty$ as $U_{avg} \to 0$.

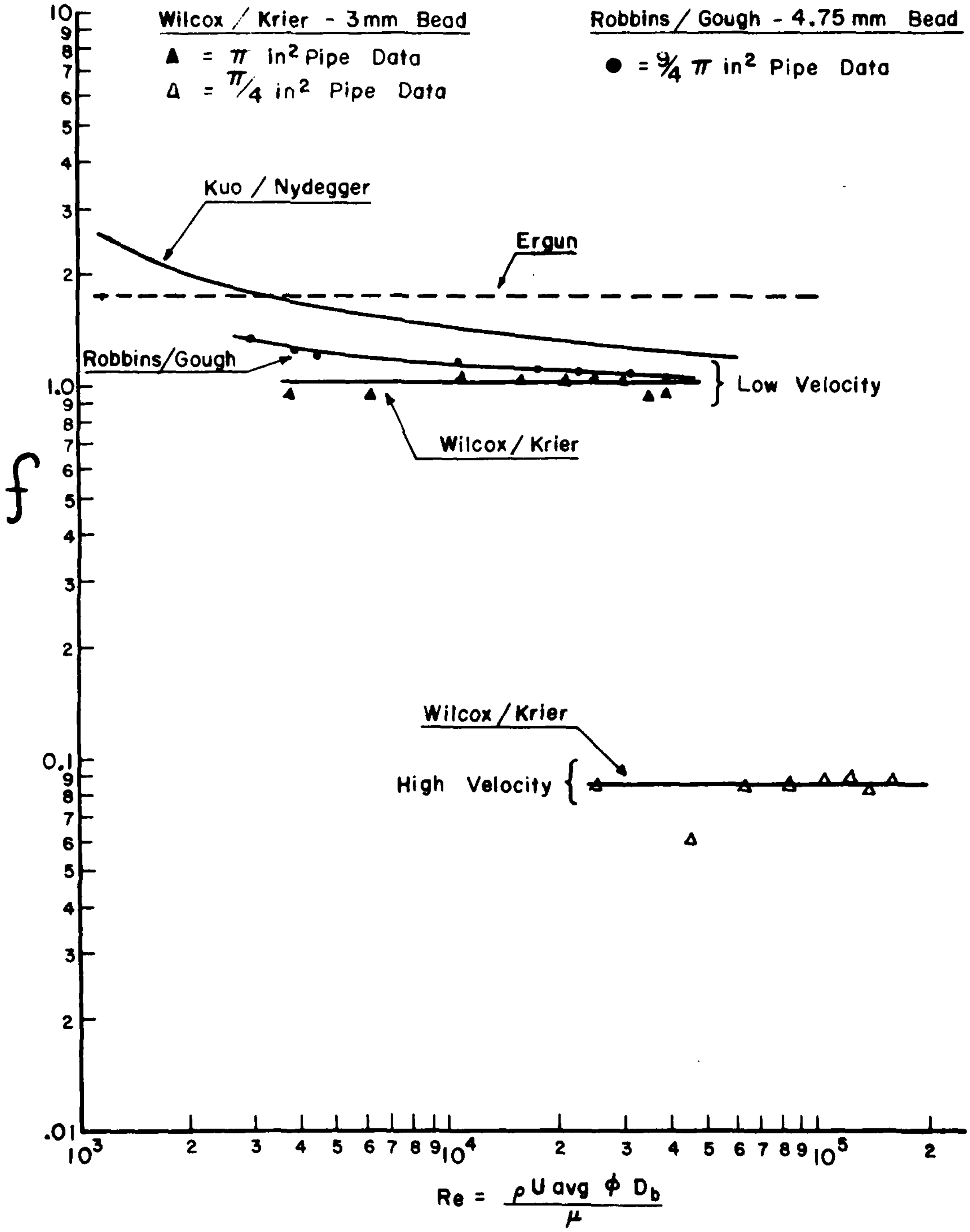

Figure 18. Alternate Form of Coefficient of Drag, Indicating Velocity Effect.

$$\boxed{\frac{\Delta P}{L} = \frac{a \rho \phi}{g_c}} \qquad (16)$$

Eq. (16) gives $\Delta P/L$ in units of lbf/ft^3; ρ must be given in lbm/ft^3. Recall the constant a equals 3.33×10^6 ft/sec^2.

In SI units Eq. (16) is simply expressed as

$$\frac{\Delta P}{L} = a' \rho \phi \qquad (16a)$$

where $\Delta P/L$ is in units of nt/m^3, ρ in units of kg/m^3, and a' equals 1.015×10^6 m/sec^2. Again Eq. (16) should only be utilized for $Re > 10^3$.

Equation (16) was derived from data utilizing almost exclusively uni-sized spherical particles packed randomly to provide the highest solid loadings (or lowest porosity, ϕ). The porosity range was therefore limited to $0.38 < \phi < 0.43$. As such, the relation [Eq. (16)] should not be used to indicated the sensitivity of the flow resistance as a function of solids loading.

As a matter of fact, when a bi-modal mixture of 6mm and 0.96mm beads was mixed, about 50/50 by weight, the resulting porosity was $\phi = 0.29$. For the same mass flow through the bed, (as for either the all 6mm or all 0.96mm beads), the data clearly indicated that the pressure gradient, $\Delta P/\Delta L$ was larger for the bi-modal mix, since the density of the gas was additionally larger.

That the correlation given by Eq. (16) is fairly accurate can be seen by reviewing the data for $\Delta P/\Delta L$ given in Figure 19, where the equation is compared to the measure pressure drop.

It should be noted that there is some similarity between our Eq. (16) and the standard fluidized bed equation. That is, a vertical bed becomes fluidized when a gas of lower density, than that of the bed particles,

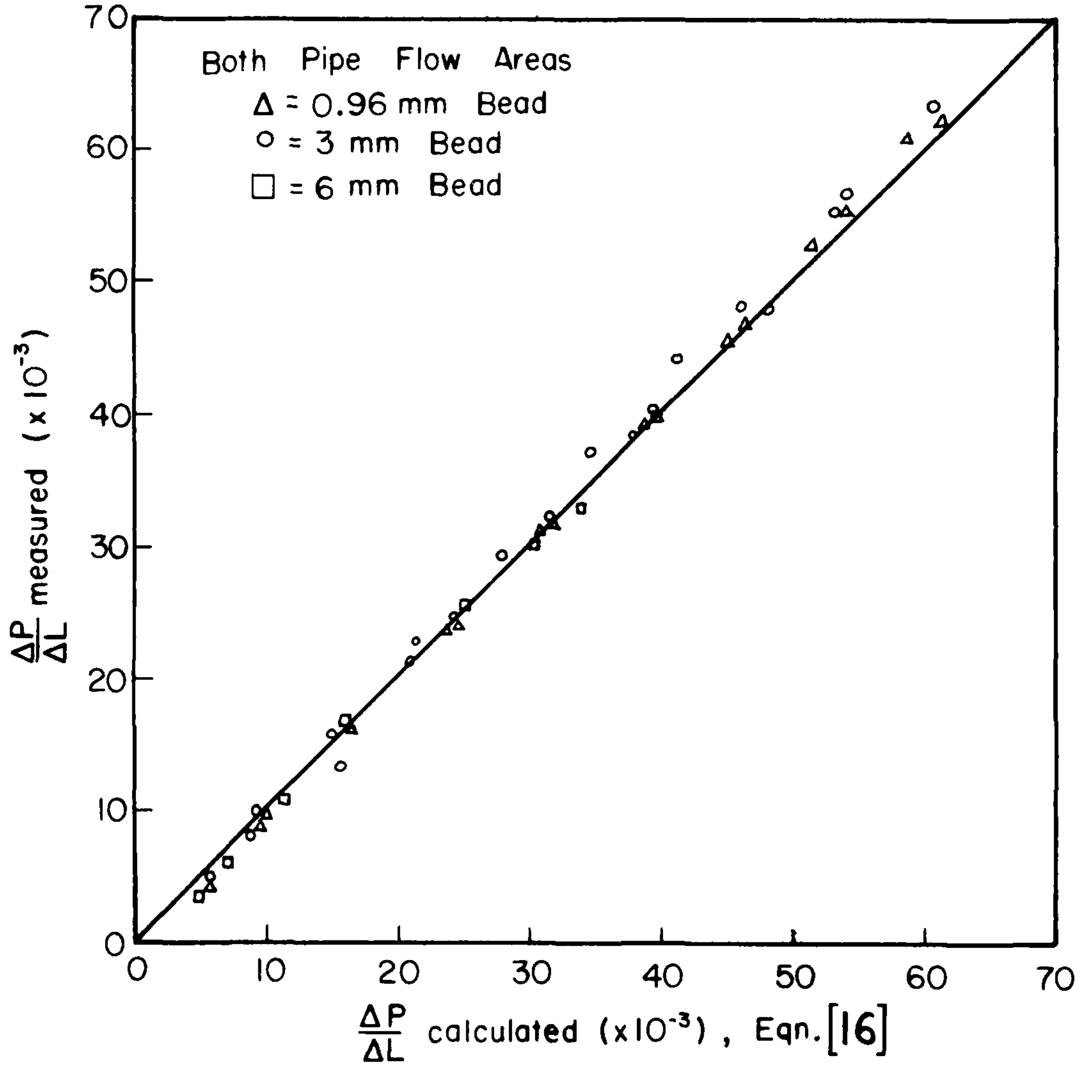

Figure 19. Comparison of Measured Pressure Drop to Predicted Pressure Drop.

flows upward through the bed causing the particles to no longer rest on each other, but be suspended by the upward force of the gas. As the gas velocity increases, the particles will expand. This fluidized state is expressed by the following equation [11],

$$\frac{\Delta P}{\Delta x} = g\ [\phi \rho_g + (1-\phi)\rho_b] \qquad (17)$$

The horizontal packed bed in this work did not become fluidized because it was tightly packed and then the bed was retained by metal disks at each end of the test section. Much more analysis would be necessary in order to explain the correlation obtained at high velocities [Eq. (16)] to a similar correlation for fluidized beds [Eq. (17)].

As one can see from Eq. (16), the pressure gradient is proportional to the average gas density in the test section. Rearranging Eq. (16), yields

$$\Delta P/\Delta x = \frac{a\ \rho\ \phi}{g_c} = C_1 P \qquad (18)$$

where $C_1 = a\phi/g_c\ RT$, which is approximately constant since the gas temperature, T_1, varies only by one or two degrees in the region where the pressure is measured. Integrating Eq. (18) gives

$$\ell n\ P = C_1 x \qquad (19)$$

Figure 20 is a plot of Eq. (19), and it can be seen that the slope, C_1, is constant independent of initial gas pressure. In fact, the slope will be constant irregardless of the bead diameter and test section used. Figure 21 graphically illustrates this point. A plot of Robbin's and Gough's data in the form of Eq. (19) yields the same results, as shown in Figure 22 [12].

Further Analysis of Developed Correlations

From Bird, Stewart and Lightfoot [4] for steady flow where Dary's

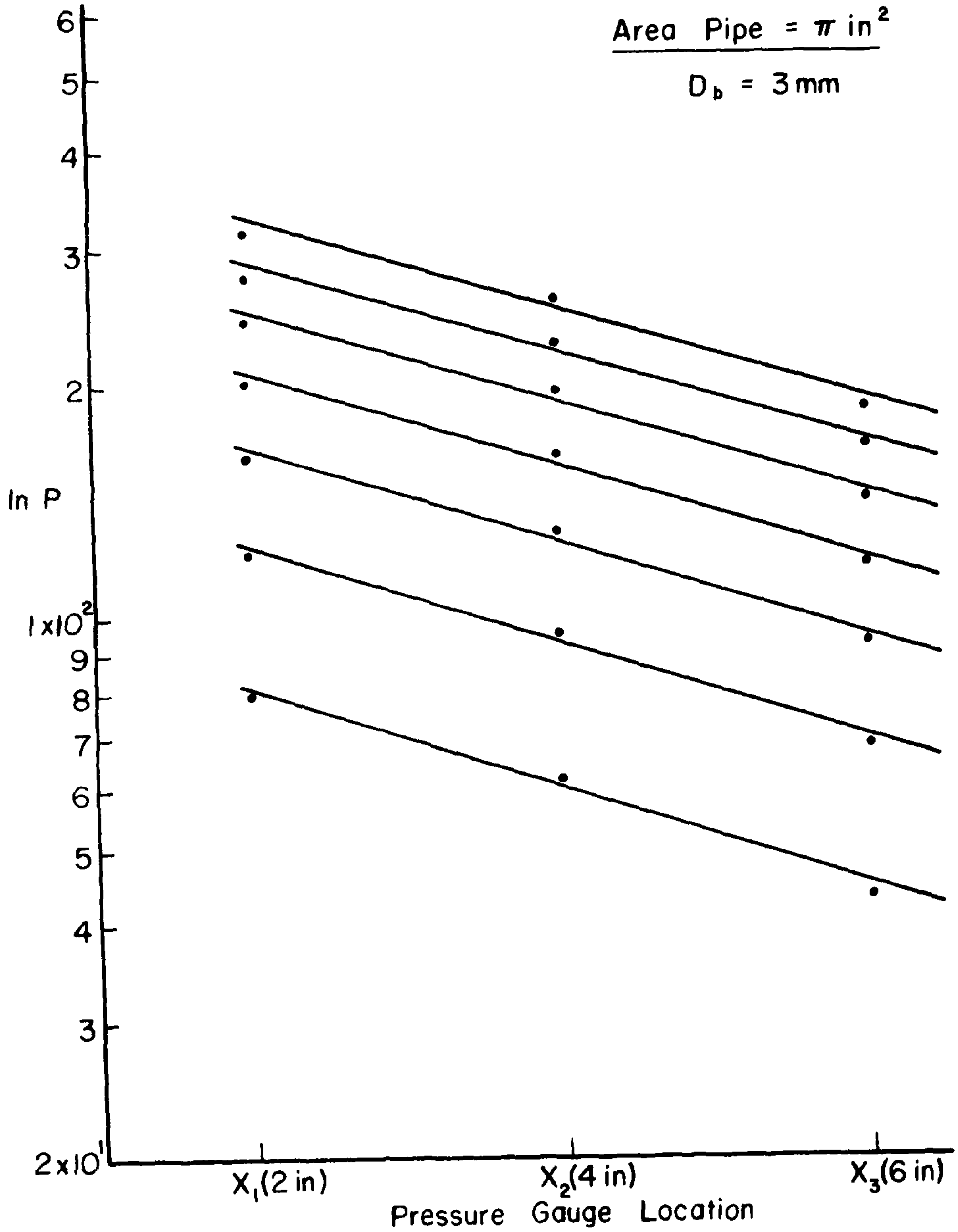

Figure 20. Constant Slope Independent of Initial Gas Pressure.

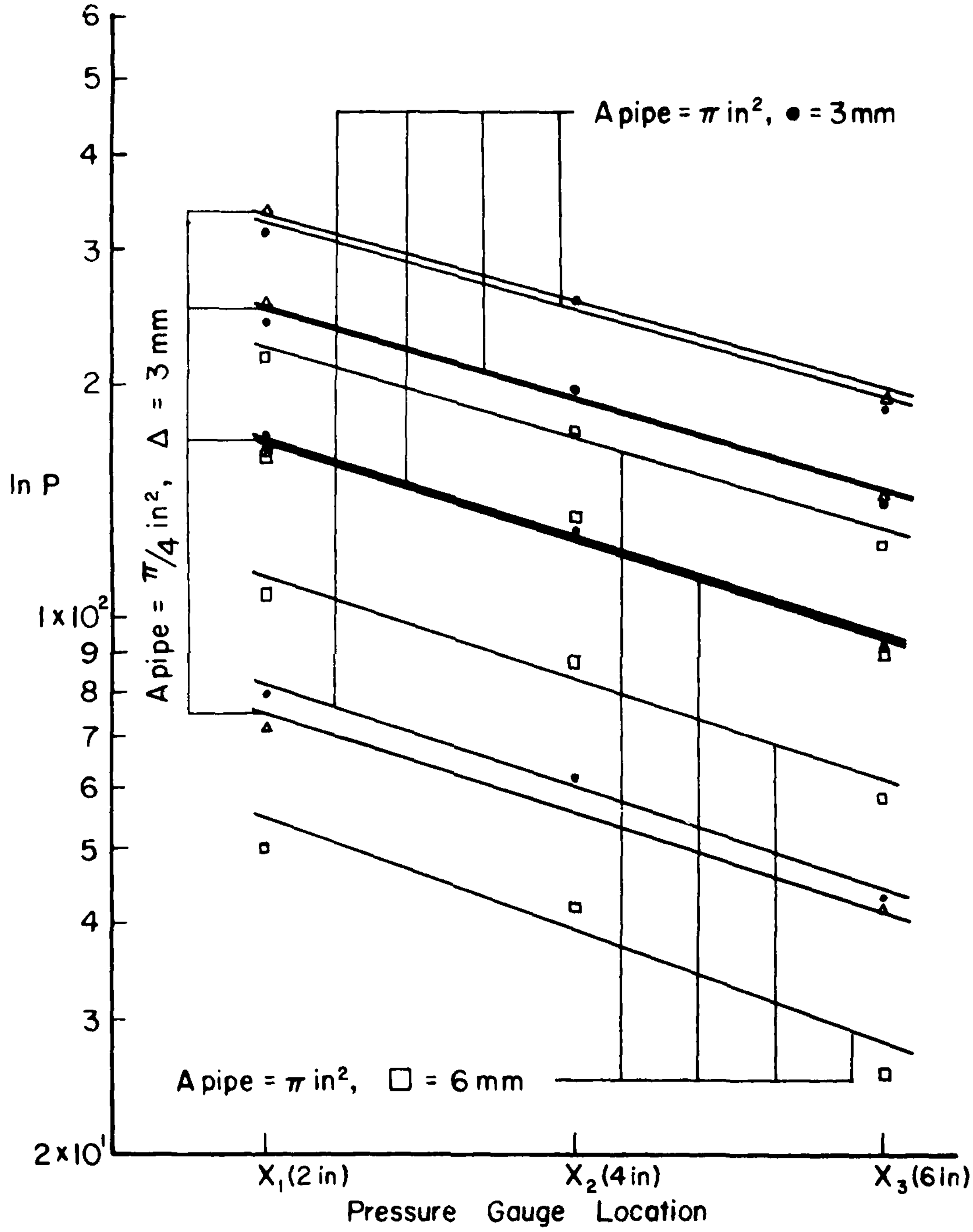

Figure 21. Constant Slope Independent of Bead Size and Test Section.

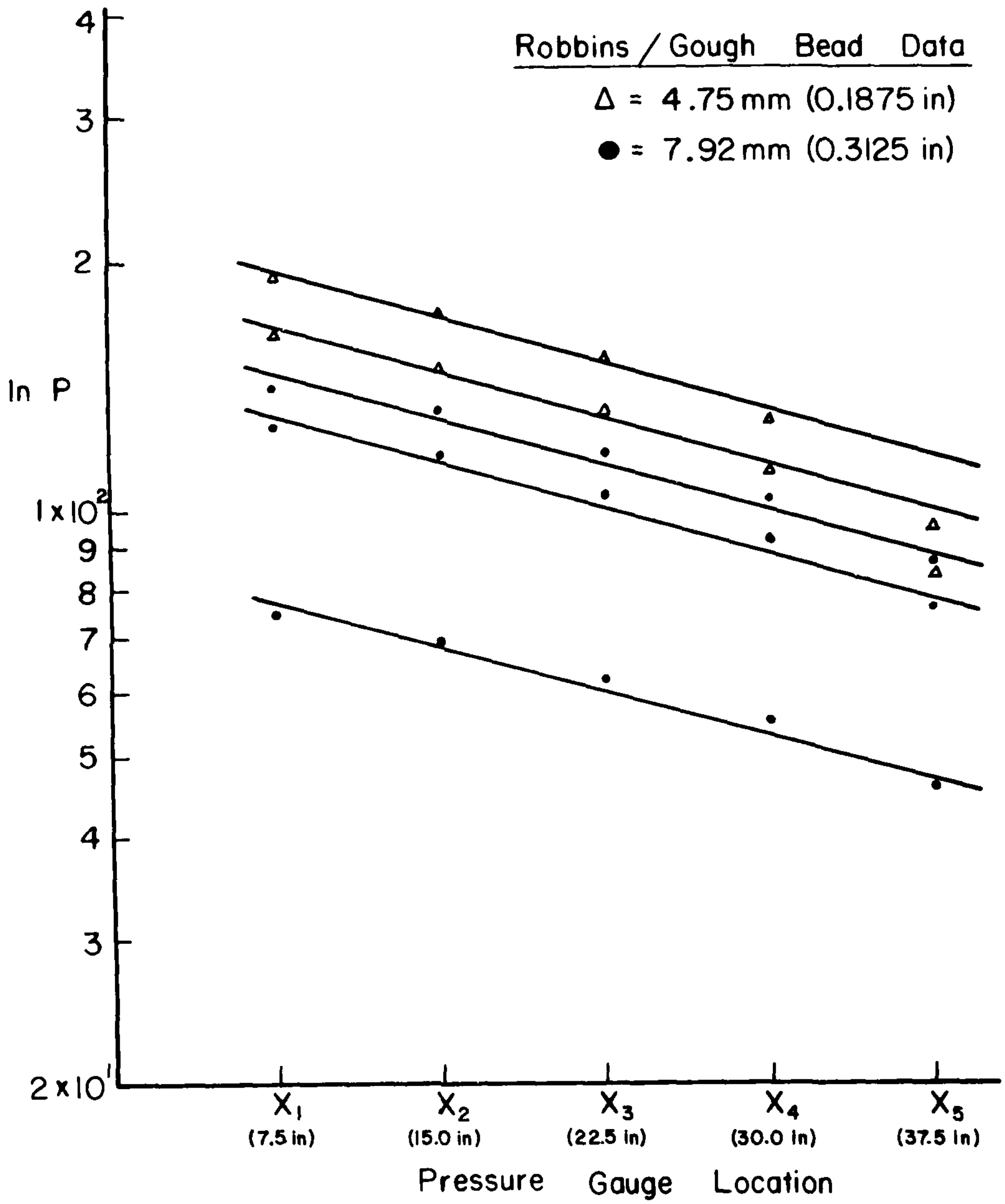

Figure 22. Constant Slope Independent of Bead Size.

Law for gas permeability is assumed valid, (low Reynolds number range), one can show that for steady isothermal gas flow

$$\nabla^2\rho^2 = 0 \quad \text{or} \quad \nabla^2 P^2 = 0 \tag{20}$$

which for one dimensional flow implies

$$P \sim \sqrt{x} \tag{21}$$

To determine how P should vary with distance, for the moderate Reynolds number flows, where the coefficient of friction

$$F_v = a + b\,Re \quad \text{or} \quad F_v \approx C_3\,Re \tag{22}$$

one can substitute Eq. (22) into (12) to get

$$\frac{dP}{dx} = C_3 Re \; \frac{\mu\, U_{avg}}{D_b^{\;2}} \tag{23}$$

and since,

$$U_{avg} = \frac{\dot{m}}{\rho\, A_{pipe}\, \phi} \quad \text{and} \quad Re = \frac{\dot{m}}{A_{pipe}} \; \frac{D_b}{\mu}$$

then simplifying Eq. (23) yields

$$\frac{dP}{dx} = C_4 \,\frac{1}{P} \tag{23a}$$

where $C_4 = C_3 \dot{m}^2\, RT/A^2_{pipe}\, \phi\, D_b$, and integrating Eq. (23a) gives

$$P^2 = C_5 X \quad \text{or} \quad P \sim \sqrt{x} \tag{23b}$$

as indicated above in Eq. (21). The expression, Eq. (23a), assumes mass flow ($\dot{m}$) is an independent parameter. If instead one assumes that $\dot{m} \sim P$, which was the case in this work, then Eq. (23) becomes, after integration,

$$\ell n\, P = C_6 X \tag{24}$$

which is the same form obtained in Eq. (19). In conclusion, the pressure

gradient, as expressed in Eq. (16) and the coefficient of drag as expressed in Eq. (15) are logical formulations for these expressions at high Reynolds numbers.

Transient Experiments

As discussed in Chapter 2 the transient tests were conducted by emptying high pressure air into the test section from a standard commercial tank. It was found that the time for this decay transient was 2.70 to 3.0 minutes. Appendix E shows why this was so. The time period for a progressive transient experiment ranged from 1.5 to 5.3 seconds. Both the decay and progressive transients were much longer than the desired millisecond time transients.

The transient tests were conducted using only the two inch test section. The resulting flow resistance for the progressive transient tests varied only slightly from the steady state tests, as shown in Figure 23. With the available data one can conclude that the derived formula for the coefficient of drag, Eq. (15), and pressure drop, Eq. (16), will accurately predict the transient results. This can be explained by comparing the total flow transient period, which ranged from 1.5 to 5.3 seconds, with a characteristic "time", Γ_1, defined as, $\Gamma_1 = \Delta x/U_{avg}$. The distance Δx is 1/6 foot (pressure gauge separation), and with U_{avg} ranging from 80 fps to 122 fps, Γ_1 ranges from 2 milliseconds to 1.36 milliseconds. Unless the flow experiment could be carried out to change the pressures significantly in time periods of the order of Γ_1, one should expect that the correlations developed in these (steady-state) experiments would be valid for moderately transient conditions.

Additional Tests with Various Size Particles

A mixture of 6mm beads and 0.96mm beads was tested. The mixture

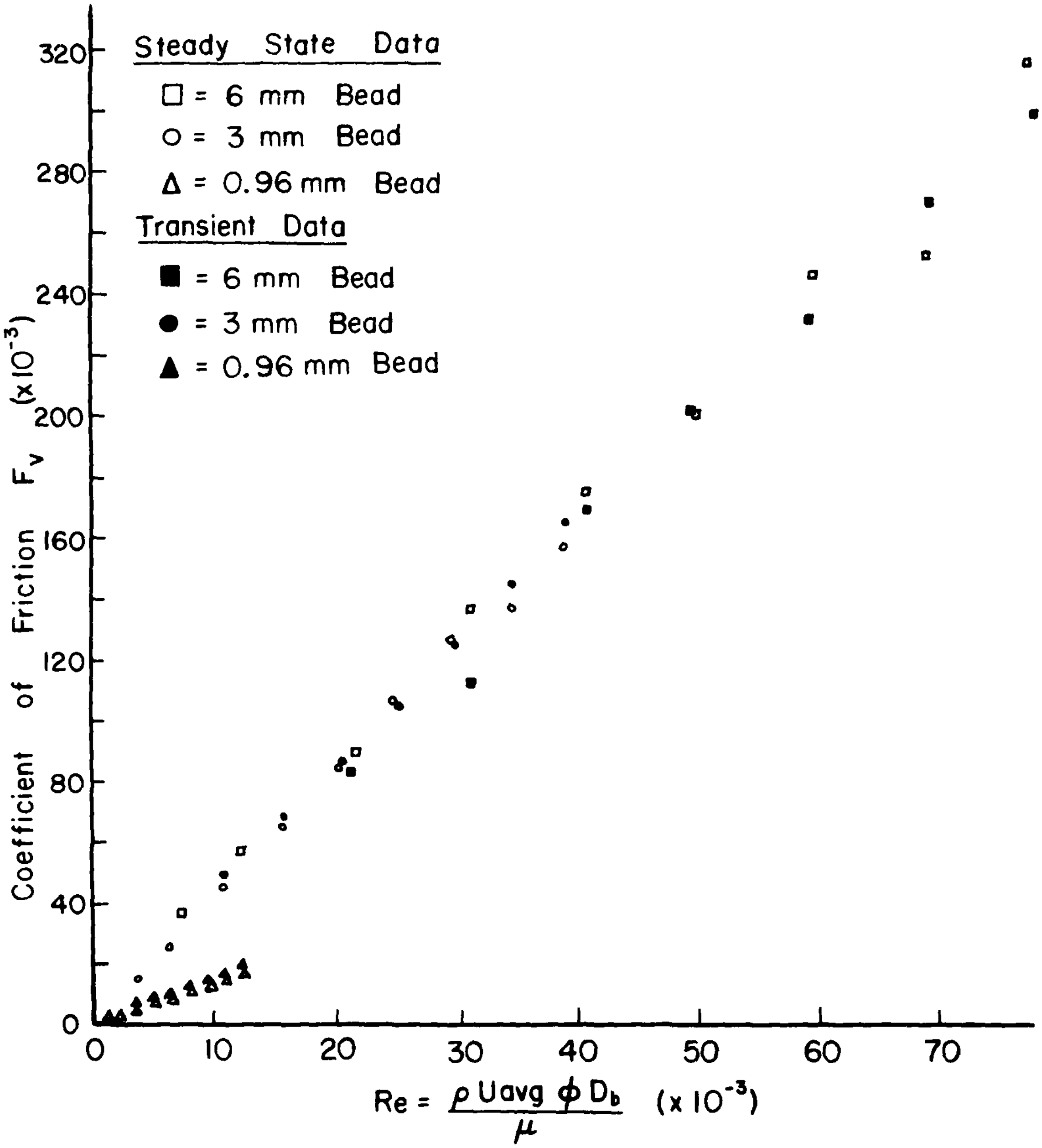

Figure 23. Comparison of Transient and Steady-State Data.

contained 50.6%, 6mm beads, and 49.4%, 0.96mm beads, by weight. The effective diameter‡ of the mixture particles was 1.249mm (0.049 in.). The porosity of this mixture was 0.2962 which indicates that the 0.96mm beads filled the voids between the 6mm beads causing a very tight packing of the particles. A plot of F_v versus Reynolds number for this mixture gave a line which was slightly above that for the 0.96mm bead, which one would expect since the effective diameter of the particles was larger.

Ottawa Sand was also packed into the two inch test section. The effective diameter of the sand was 0.7315mm (0.0287 in.). A plot of the resulting F_v versus Reynolds number, gave a line slightly below that for the 0.96mm bead, which was shown in Figure 14a.

The results of the mixture and sand tests, indicate that the 0.96mm bead data is accurate. Also, the equations for F_v and pressure gradient, (15) and (16) respectively, would correctly predict the results of the above tests.

Finally, a test was carried out in the two inch test section using a packed bed of cylindrical shaped solids, 10.23mm (0.4028 in.) long and 4.65mm (0.183 in.) in diameter. The resulting values of the coefficient of drag, F_v, when plotted versus Reynolds number, are in agreement with the results Robbins and Gough [6] obtained, if an effective diameter of D_b = 0.183 inch is used.

---

‡ $D_b \text{ (effective)} = 2\left[\frac{(1-\phi_{bed})}{(1-\phi_i)} \times \frac{N_i}{N_{Total}} \times r_{bi}^3\right]^{1/3}$

where N = number of particles.

Future Work Required

The formulated correlation to predict pressure drop, Eq. (16) [$\Delta P/L = a\ \rho\ \phi/g_c$], was compared to some actual pressure gradient data from Robbin's and Gough's work [12]. It was found that the value of a for their data was 2.56×10^6 ft/sec^2 instead of 3.33×10^6 ft/sec^2 as developed in this work. Hence, the predicted pressure gradients were 23% higher than the measured pressure gradients at their high Reynolds number range (Re $\simeq 80 \times 10^3$).

In light of these results, further work should be conducted in order to test the validity of the correlations for the coefficient of drag, Eq. (15), and the pressure gradient, Eq. (16). This would entail constructing an additional three inch test section and obtaining a pressure reservoir which would increase the inlet pressure to the packed bed by at least an order of magnitude. To fabricate the high pressure vessel of a significant capacity, here at the University of Illinois, as well as the purchase of a compressor that could replenish the reservoir in the order of several thousand pounds per square inch, would require a substantial investment.

An alternate method of increasing the pressure in the test section, is to manifold several commercial gas bottles and reduce the nozzle's throat area, resulting in a high stagnation pressure in the plenum tank and high pressures in the test section. Tests would be conducted over the same Reynolds number range, but with higher pressures. For safety reasons this was not attempted.

Conclusions

The work reported here indicates that in gaseous flow through packed beds, Ergun's [1] correlation is valid for Reynolds number less than 1400.

As the Reynolds number increases, there is a large deviation of his extrapolated results from the actual pressure drop through the packed bed.

In fact, at high Reynolds numbers, 10^4 - 10^5, it has been shown that the coefficient of drag is no longer a sole function of Reynolds number, but a function of bead diameter and velccity, other than the velocity effect in the Reynolds number. It has graphically been illustrated, (as shown in Figure 16) that irregardless of the flow area of the packed bed, the predicted coefficient of drag, Eq. (15), accurately correlates the measured friction factor (F_V) for whatever size particle the bed is composed of.

Further, at high Reynolds number, the pressure gradient within a packed bed is a function, solely, of the average gas pressure, (or density), in the bed. This pressure gradient is accurately predicted using Eq. (16).

It must be emphasized that the formulated correlation for the coefficient of drag, Eq.(15), and the pressure gradient, Eq. (16), were developed for high velocity (and high Reynolds numbers). These correlations are not applicable for a Reynolds number realem less than 10^3. Additional work is now in order to develop an additional correlation that will provide the transition equation from the relatively low velocity (and lower Reynolds number) conditions, as developed by either Ergun or Kuo and Nydegger, to the conditions tested here.

References

1. Ergun, S., "Fluid Flow Through Packed Columns," Chemical Engineering Progress, 48(2): pp. 89-94, February 1952.

2. Benenati, R. and Brosilow, C., "Void Fraction Distribution in Beds of Spheres," A.I. Chemical Engineering Journal, 8(3): pp. 359-361, July 1962.

3. Ergun, S. and Orning, A. A., Industrial Engineering Chemistry, 41, p. 1179, 1949.

4. Bird, R, Stewart, W. and Lightfoot, E., Transport Phenomena. New York: John Wiley and Sons, Inc., 1966.

5. Kuo, K. K. and Nydegger, C. C., "Flow Resistance Measurement and Correlation in a Packed Bed of WC 870 Ball Propellants," Journal of Ballistics, 2(1): pp. 1-25, 1978.

6. Robbins, R. and Gough, P. S., "An Experimental Determination of Flow Resistance in Packed Beds of Gun Propellant," Proceedings of 15th JANNAF Combustion Meeting, CPIA pub. 297, September 1978.

7. Krier, H., Gokhale, S. S. and Hoffman, S. J., "Flow Analysis Applied to Deflagration-to-Detonation Transition," AIAA Paper No. 78-1013, presented at the AIAA/SAE 14th Joint Propulsion Conference, Las Vegas, NV, July 1978.

8. Krier, H. and Kezerle, J. A., "A Separated Two-Phase Flow Analysis to Study Deflagration-to-Detonation Transition (DDT) in Granulated Propellant," Seventeenth International Symposium on Combustion. The Combustion Institute, Pittsburgh, PA, 1979.

9. "Fluid Meters," American Society of Mechanical Engineers, 6th edition: p. 180, 1971.

10. Johnson, R. C., Real Gas Effects in Critical Flow Through Nozzles and Tabulated Thermodynamic Properties, NASA TN D-2565, 1965.

11. Wallis, G. B., One-Dimensional Two Phase Flow. New York: McGraw-Hill Book Company, 1969.

12. Personal communication with Fred Robbins, Naval Ordnance Station, Indian Head, MD, February 1980.

APPENDIX A

REDUCTION FORMULA

Robbins and Gough [Reference 6] were able to obtain pressure drop data, for high pressure flow through packed beds of various sized particles. Knowing the mass flow rate, porosity, Reynolds number and size particle, they were able to compute a friction factor from the following equation

$$\hat{F}_s = \frac{(P_j^{\,2} - P_i^{\,2})\ \phi^3\ A^2 D_b\ g_c}{2(1-\phi)\ \dot{m}^2\ \ RTL} \tag{A-1}$$

where

$\hat{F}_s$ = friction factor

P_i, P_j = pressure at station i, j, i > j

ϕ = porosity

A = area

D_b = effective diameter of particle $(\frac{6V_b}{S_b})$

$\dot{m}$ = mass flow rate

R = gas constant

T = temperature

L = length between gages i and j

g_c = constant to reconcile units

Multiplying both sides of (A-1) by Re $\frac{(1-\phi)}{\phi^2}$ where Re = $\frac{\rho_m\ \phi U_m\ D_b}{\mu}$ yields,

$$\hat{F}_s \cdot \frac{Re(1-\phi)}{\phi^2} = \frac{(P_j - P_i)}{L}\ \frac{(P_j + P_i)}{2\ RT}\ \frac{\phi\ A^2\ D_b\ g_c}{\dot{m}^2} \cdot \frac{\rho_m\ \phi U_m D_b}{\mu} \tag{A-2}$$

Now, mass flow $\dot{m} = \rho_m\ \phi U_m\ A$ (A-3)

Pressure drops $\Delta P = P_j - P_i$ (A-4)

Average density $\rho_m = \dfrac{(P_j + P_i)}{2\ RT}$ (A-5)

Average velocity $U_m = (U_g - U_p)$ (A-6)

Substituting equations (A-3) through (A-6) into equation (A-2) yields

$$\hat{F}_s \cdot Re\frac{(1-\phi)}{\phi^2} = \frac{\Delta P}{L}\ \frac{D_b^2\ g_c}{\mu\ U_m} \tag{A-7}$$

solving for $\Delta P/L$

$$\frac{\Delta P}{L} = \hat{F}_s \cdot \frac{\mu\ U_m}{D_b^2\ g_c} \cdot Re\ \frac{(1-\phi)}{\phi^2} \tag{A-8}$$

hence

$$\frac{\Delta P}{L} = \frac{\mu(U_g - U_p)}{D_b^2} \cdot \frac{(P_j^2 - P_i^2)\phi\ A^2\ D_b\ Re}{2\dot{m}^2\ RTL\ g_c} \tag{A-9}$$

APPENDIX B

NOZZLE

The American Meter Sonic Flow nozzle provides sonic flow at the throat of the nozzle, and supersonic flow at the exit of the nozzle, and in the test section when empty. This fact was confirmed by running a test at 400 psig through an empty test section and recording the dynamic pressures.

The nozzle as purchased has an exit diameter to throat diameter ratio of 0.6875 to 0.3750 inches, or an area ratio, $\frac{Ae}{A^*} = 3.361$. For ideal isentropic choked flow, Ae/A* and Pe/Po are related by

$$Ae/A^* = \frac{\Gamma}{\left(\frac{Pe}{Po}\right)^{1/\gamma}\sqrt{\frac{2\gamma}{\gamma-1}\left[1-\left(\frac{Pe}{Po}\right)^{\frac{\gamma-1}{\gamma}}\right]}} \qquad \text{(B-1)}$$

where $\Gamma = \sqrt{\gamma}\left(\frac{2}{\gamma+1}\right)^{\frac{\gamma+1}{2(\gamma-1)}}$

Solving Eq. (B-1) implicitly, one determines that Pe/Po = 0.03916, and hence Pe = 16.23 psia.

We in fact measured 17.62 psia, 16.37 psia, and 16.37 psia, at gauges 1, 2, and 3 respectively. The differences in the actual and ideal pressure, 16.23 psia, were due to the real gas effects not being taken into account. In addition, the low gauge pressures recorded on the gauges were about 2.0 psig, and noting at ± 0.5 psig accuracy of the gauges, this would also account for the small discrepancies.

Now $\frac{Pe}{Po}$ and Mach number are related for isentropic flow by

$$\frac{Pe}{Po} = \frac{1}{[1 + \frac{\gamma-1}{2}M^2]^{\gamma/\gamma-1}} \qquad \text{(B-2)}$$

Solving Eq. (B-2) for M, gives one the Mach number in the test section, M = 2.76.

When the test section is packed, the flow can no longer remain supersonic, but in fact is reduced to subsonic velocities. At a test pressure of 400 psig, with a packed test section the average velocity in the test section is determined by mass flow, i.e.,

$$\frac{\dot{m}}{\rho_m \; \phi \; A} = U_{avg} \qquad \text{(B-3)}$$

$$\text{where} \quad \rho_m = \frac{P_1+P_2+P_3}{3RT_{T.S.}} \qquad \text{(B-4)}$$

giving an average gas velocity U_{avg} of 124.876 ft/sec.

and

$$M = \frac{U_{avg}}{\sqrt{\gamma RT_{T.S.}}} \qquad \text{(B-5)}$$

yields $M_{Test\ Section} = 0.11$

Hence, the sonic nozzle provides supersonic flow prior to the packed test section, but once the flow enters the test section the drag reduces the velocity to subsonic flow.

The purpose of utilizing the supersonic nozzle is to assure choked flow through an isentropic contriction so that the mass flow can easily be calculated from the relation

$$\dot{m} = C^* \; Po \; A^* \; / \; \sqrt{RT_o} \qquad \text{(B-6)}$$

where $C^* = \Gamma \cdot C_D$, and C_D is an effective discharge coefficient.

Equation (B-6) includes a non-ideal correction coefficient, C*, to the classical choked flow equation as given in Reference 10.

When calculating the mass flow through the sonic flow nozzle, real gas effects must be taken into account. In accordance with Johnson [10], it has been found that real gas effects cause definite corrections in the ideal gas, isentropic flow, calculations for mass flow through a nozzle. Johnson has tabulated a Critical Flow Factor, C*, which takes into account the compressibility and real gas effects for mass flow through a nozzle, with throat area A*, upstream temperature, T_o, and pressure, P_o, and $R = \frac{\overline{R}}{MW} = 53.32 \frac{lbf\text{-}ft}{lbm\text{-}^\circ R}$, for air.

$$\dot{m} = \frac{A^* C^* P_o}{\sqrt{RT_o}} \tag{B-7}$$

For ideal isentropic flow, theoretical

$$C^* = \Gamma = \sqrt{\gamma}\left(\frac{2}{\gamma+1}\right)^{\frac{\gamma+1}{2(\gamma-1)}} = 0.6847 \text{ if } \gamma = 1.4 \tag{B-8}$$

Johnson showed that the critical flow factor varies with the plenum stagnation pressure and temperature from 0.684 to 0.770 which is a 12% variation from the theoretical ideal gas critical flow factor of 0.6847.

APPENDIX C

CALIBRATION

The Bourdon gauges were calibrated by using a Refinery Supply Co., Model 3S260, dead weight tester. A weight was applied to the dead weight tester which subsequently applied a pressure to the Bourdon gauge. The respective gauge reading was recorded. A plot of the gauge reading versus the applied pressure was prepared for each Bourdon gauge. This gave a calibration curve for each Bourdon gauge.

A similar process was followed with the Setra System Transducers, however, the output from the gauge was recorded on a voltmeter and also an oscilloscope. Figure C1 shows the oscilloscope calibration display. Two calibration curves were constructed for each transducer, one for the oscilloscope, and the other for the voltmeter. On these curves the pressure was plotted versus the voltage.

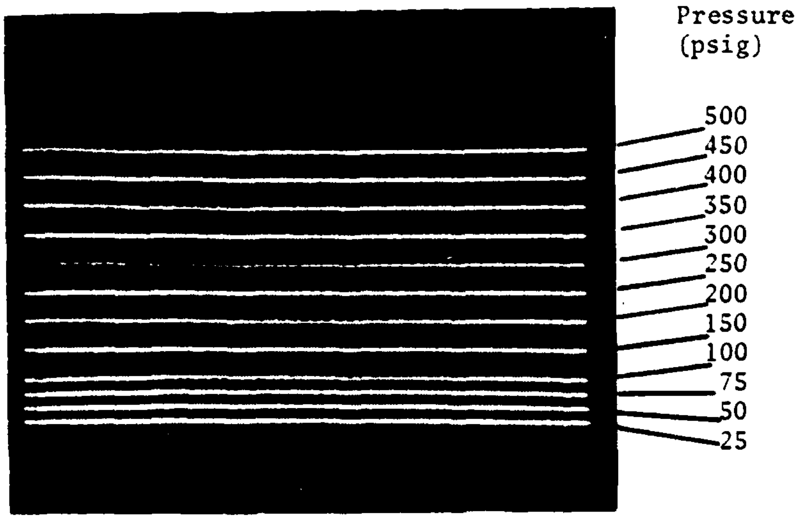

Figure C1. Oscilloscope Calibration Display

APPENDIX D

TEST PROCEDURES

It is imperative that the same test procedures are followed for every test, both steady state and transient, so that the resulting data can be accurately compared. For the steady state tests, the procedure is numerated below.

Steady State

1. Close Grove Regulator
2. Turn on main air supply
3. Turn on oscilloscope (voltmeters) and storage facility
4. Power to thermocouple amplifier
5. Power to pressure transducer amplifiers
6. Remove test section from apparatus
7. Pack test section with appropriate size beads
8. Replace test section
9. Compress bed with air pressure that is higher than any test pressure that will be used.
10. Adjust scope to zero output
11. Erase oscilloscope
12. Have oscilloscope camera ready
13. Open grove regulator to the desired test pressure
14. Run for 60 seconds. Recording pressure on Bourdon gage 2 and thermocouples 1, 2 and 3.
15. Close Grove Regulator
16. Inspect oscilloscope stored display for any fluctuation in trace, indicating unsteady flow.
17. Take picture of stored traces on oscilloscope
18. Erase and zero scope
19. Make run at next higher pressure, starting at step 11.

In the transient test, the test apparatus is modified as explained in Chapter 2. The test procedures are listed below.

Transient

1. Close Grove Regulator
2. Turn on main air supply
3. Turn on oscilloscope and activate storage facility
4. Power to thermocouple amplifier
5. Power to pressure transducer amplifiers
6. Remove test section from apparatus
7. Pack test section with beads
8. Replace test section
9. Compress bed with air pressure from the 9 tank bank, same as in steady state case.
10. Adjust scope to zero output
11. Erase oscilloscope screen
12. Have oscilloscope camera ready
13. Ensure ball valve is closed
14. Open compressed air bottle valve
15. Activate sweep of oscilloscope and open ball valve simultaneously
16. Let air bottle empty until pressure in plenum drops below 100 psig, then close ball valve.
17. Continuously monitor temperature in plenum tank.
18. Stop sweep of scope
19. Take picture of stored traces on oscilloscope
20. Erase and zero scope
21. Repeat procedure with new air bottle and a different size bead

APPENDIX E

TRANSIENT CHAMBER EMPTYING

In order to calculate the transient decay of pressure within a tank of gas, one must start with a tank of volume V_o, initial pressure P_o, and initial temperature T_o. The gas is specified by the gas constant R and specific heat ratio γ. Assume that the pressure in the tank is uniform (no waves), $P_a < P_o$, and $\frac{P_a}{P_o} \leq \left(\frac{2}{\gamma+1}\right)^{\frac{\gamma}{\gamma-1}}$ (flow is choked). For choked flow,

$$\dot{m} = \frac{P\ A^*\ \Gamma}{\sqrt{RT}} \qquad \text{(E-1)}$$

where $\Gamma = \sqrt{\gamma}\ \left(\frac{2}{\gamma+1}\right)^{\frac{\gamma+1}{2(\gamma-1)}} = 0.6847$ (for air)

Now, also

$$\dot{m} = -\frac{dM}{dt} \qquad \text{(E-2)}$$

$$-\frac{dM}{dt} = -\frac{d}{dt}(\rho v) = -v\ d\rho/dt \qquad \text{(E-2a)}$$

Assume isentropic expression:

$$\frac{P}{P_o} = \left(\frac{\rho}{\rho_o}\right)^{\gamma} \quad \text{and} \quad \frac{T}{T_o} = \left(\frac{P}{P_o}\right)^{\frac{\gamma-1}{\gamma}} \qquad \text{(E-3)}$$

thus $$d\rho = \frac{1}{\gamma}\left(\frac{\rho_o}{P_o}\right) dp \qquad \text{(E-4)}$$

$$d\rho = \frac{dp}{dt}\left[\frac{p\rho_o}{(\rho/\rho_o)^{\gamma}}\right]\frac{1}{\gamma} \qquad \text{(E-4a)}$$

and from (E-2a)

$$-\frac{dM}{dt} = \frac{v}{\gamma}\left[\frac{\rho_o}{(P_o)^{1/\gamma}}\right]\left[P^{\frac{1-\gamma}{\gamma}}\right]\frac{dp}{dt} \tag{E-5}$$

Substituting equation (E-1) for the left hand side of (E-5) yields,

$$\frac{A^* \, \Gamma \, P}{\sqrt{RT}} = -\left[\frac{v}{\gamma}\frac{\rho_o}{(P_o)^{1/\gamma}}\right] P^{\frac{1-\gamma}{\gamma}} \frac{dp}{dt} \tag{E-6}$$

Multiplying (E-6) by P_o/P_o and substituting equation (E-3), $T/T_o = (P/P_o)^{\frac{\gamma-1}{\gamma}}$, into (E-6) yields,

$$\frac{P_o(\Gamma/\sqrt{R})\ A^*}{\sqrt{T_o}}\left(\frac{P}{P_o}\right)^{[1-(\frac{\gamma-1}{2\gamma})]} = -\frac{v}{\gamma}\ \rho_o\left(\frac{P}{P_o}\right)^{\frac{1-\gamma}{\gamma}}\frac{d(P/P_o)}{dt} \tag{E-7}$$

Substituting the state equation, $P_o = \rho_o RT_o$, into (E-7), one obtains,

$$\Gamma\ A^* \sqrt{RT_o} = -\frac{v}{\gamma}\left(\frac{P}{P_o}\right)^{\frac{1-3\gamma}{2\gamma}}\frac{d(P/P_o)}{dt} \tag{E-8}$$

Now define $\hat{P} = P/P_o$ and rearrange (E-8)

$$\frac{d\hat{P}}{dt}\left[\frac{v/A^*}{\gamma\sqrt{RT_o}\ \Gamma}\right] + \hat{P}^{\frac{3\gamma-1}{2\gamma}} = 0 \tag{E-8a}$$

Define $\tau_{res} = \dfrac{v/A^*}{\gamma\ \Gamma\sqrt{RT_o}}$ (units of sec.) (E-9)

and $\hat{t} \equiv t/\tau_{res}$ (nondimensional) (E-9a)

Thus $\dfrac{d\hat{P}}{d\hat{t}} + (\hat{P})^{\frac{3\gamma-1}{2\gamma}} = 0$ (E-10)

with initial conditions $\hat{t} = 0$, $\hat{P} = 1$

Solving equation (E-10) yields

$$-\hat{t} = \frac{\hat{P}^{1-n}}{1-n} + C \qquad \text{(E-11)}$$

where $n = \frac{3\gamma-1}{2\gamma}$ and C = constant

Applying the initial conditions and solving for the constant in equation (E-11) gives

$$C = -\left(\frac{1}{1-n}\right) \qquad \text{(E-11a)}$$

Hence

$$\hat{P} = [1 - (1-n)\,\hat{t}]^{\frac{1}{1-n}} \qquad \text{(E-12)}$$

For $\gamma = 1.4$ (air) equation (E-12) becomes

$$\hat{P} = [1 + (\tfrac{1}{7}\;\hat{t})]^{-7} \qquad \text{(E-13)}$$

or

$$\hat{t} = 7\,[\hat{P}^{-1/7} - 1] \qquad \text{(E-14)}$$

For our specific case the air bottles that are being used have a volume $v = 309\ ft^3$, $P_o = 2414.7$ psia, $T_o = 530°R$, $R = 53.3\ \frac{lbf\text{-}ft}{lbm°R}$, and $\gamma = 1.4$. In order to empty the gas bottle until conditions become unchoked ($P_o = 27.84$ psia), then $\hat{P} = \frac{27.84}{2414.7} = .0115$, and $\hat{t} = 6.248$. Therefore, it takes 2.73 minutes (164 seconds). Figure E-1 is a graph of nondimensional pressure versus nondimensional time.

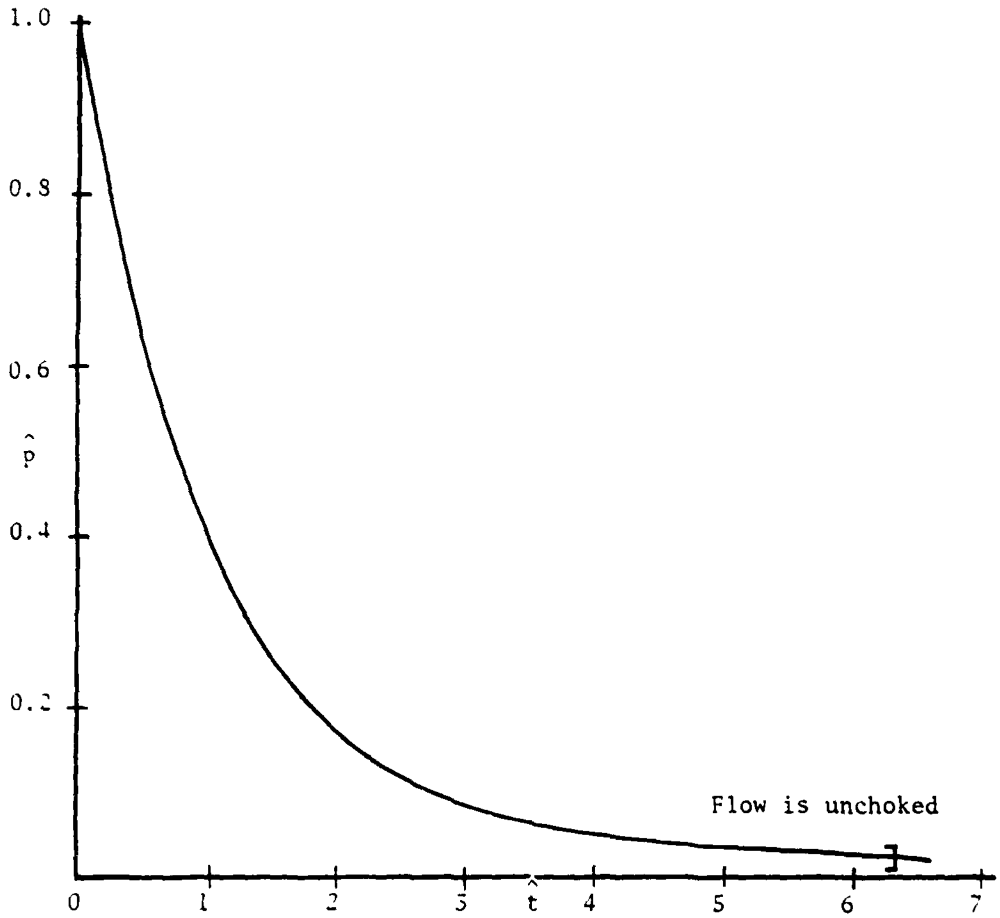

Figure E-1. Nondimensional Transient Decay of Pressure within a Tank.

APPENDIX F

REDUCTION OF EXPERIMENTAL DATA

The experimental data was collected as stated in Chapter 2. The pressure transducer readings from the voltmeters were recorded in units of volts. The transducer calibration charts were then used to convert the voltmeter readings to pressure. The steady state pressure readings on Bourdon Gauges 1 and 2 were recorded on the data sheet, as well as the thermocouple readings at position 1, 2, and 3. A typical data sheet is shown in Figure F-1.

Bourdon Gauge	Reading PSI	Actual PSI
1	370	368
2	100	100

Thermo-Couple	°F	°R
1	88	548
2	88	548
3	85	545

Pressure Transducer	Oscilloscope Displacement in Divisions	Volts/Div	m Volts	Pressure Psi
1			750	79.25
2			597	61.5
3			399	43

Porosity: 0.3868 Size Beads: 3mm

Mass Flow Rate: 0.2881 lbm/sec Reynolds #: 10817.46

Figure F-1. Typical Two Phase Flow Data Sheet.

After the series of test with the specific size beads, in this case 3mm, is completed, the beads in the test section are weighted to determine their total mass. This mass is then divided by the density of the 3mm bead to compute the porosity in the test section, as shown below.

Mass of 3mm beads: 657.447 grams.

$$\frac{\text{Mass}}{\text{density}} = \frac{657.447 \text{ grams}}{42.292 \text{ gram/in}^3} = 15.545 \text{ in}^3$$

$$\phi = 1 - \frac{\text{Vol beads}}{\text{Vol Test Section}} = 1 - \frac{15.545 \text{ in}^3}{25.352 \text{ in}^3} = .3868$$

$$\phi = 0.3868$$

The mass flow is computed using equation (B-7). Note all calculations are performed using absolute pressure.

$$\dot{m} = \frac{A^*C^*P_o}{\sqrt{RT_o}}$$

$$= \frac{(\pi \text{in}^2)(\text{ft}^2/144 \text{ in}^2)(0.68684)(114.38\text{lbf/in}^2)(144\text{in}^2/\text{ft}^2)(32.2\frac{\text{lbm-ft}}{\text{lbf-sec}^2})}{\sqrt{(53.3 \frac{\text{lbf-ft}}{\text{lbm }^\circ\text{R}})(548\ ^\circ\text{R})(32.2 \frac{\text{lbm-ft}}{\text{lbf-sec}^2})}}$$

$$\dot{m} = 0.2881 \text{ lbm/sec}$$

The average density is computed from equation (B-4) and average velocity from equation (B-3).

$$\rho_m = \frac{(P_1 + P_2 + P_3)}{3\ R\ T_{T.S.}} = \frac{[(\frac{79.25 + 61.5 + 43}{3}) + 14.38 \text{ lbf/in}^2][\frac{144 \text{ in}^2}{\text{ft}^2}]}{(53.3 \frac{\text{lbf-ft}}{\text{lbm }^\circ\text{R}})\ (548\ ^\circ\text{R})}$$

$$\rho_m = 0.3729 \text{ lbm/ft}^3$$

$$U_{avg} = \frac{\dot{m}}{\rho_m \; \phi \; A_{pipe}} = \frac{(.2881 \text{ lbm/sec})}{(.3729 \text{ lbm/ft}^3)(.3868) \; (\pi \text{ in}^2)(\text{ft}^2/144 \text{ in}^2)}$$

$$U_{avg} = 91.55 \text{ ft/sec}$$

The formula for Reynolds number is given by equation (4a)

$$Re = \rho \frac{U_m \; D_b}{\mu} = \rho \frac{U_{avg} \; \phi \; D_b}{\mu} = \frac{\dot{m}}{A_{pipe}} \; \frac{D_b}{\mu}$$

$$Re = \frac{(.2881 \text{ lbm/sec}) \; (.01003 \text{ ft})}{(\pi \text{ in}^2)(\text{ft}^2/144 \text{ in}^2) \; (1.2248 \times 10^{-5} \; \frac{\text{lbm}}{\text{sec-ft}})}$$

$$Re = 10817.46$$

The reduced experimental data for a typical test using a 3mm and 0.96mm bead in a 2 inch test section are tabulated in Table F-1.

Table F-1. Reduced Experimental Data (2 in. I.D.)

3mm Bead Data, ϕ = 0.3868

Plenum Pressure (Psi)	ΔP 1-3 (Psi)	ρ_m (lbm/ft^3)	$\dot{m}$ ($\frac{lbm}{sec}$)	U_{avg} (Fps)	Re #
25	11.25	0.1427	0.1008	83.71	3784.93
50	19.25	0.2201	0.1649	88.78	6191.81
100	36.25	0.3729	0.2881	91.55	10817.46
150	52.25	0.5354	0.4138	91.58	15536.61
200	67.75	0.6966	0.5409	92.01	20308.32
250	86.50	0.8593	0.6685	92.18	24851.42
300	102.75	1.0235	0.7944	91.97	29532.02
350	111.0	1.1967	0.9311	92.20	34614.14
400	131.5	1.3451	1.0592	93.31	38991.96

0.96mm Bead Data, ϕ = 0.3948

Plenum Pressure (Psi)	ΔP 1-3 (Psi)	ρ_m (lbm/ft^3)	$\dot{m}$ ($\frac{lbm}{sec}$)	U_{avg} (Fps)	Re #
25	10.25	0.1401	0.1020	84.53	1207.11
50	20.5	0.2267	0.1664	85.23	1969.24
100	37.25	0.3979	0.2953	86.17	3494.69
150	55	0.5803	0.4247	84.98	5026.06
200	72	0.7497	0.5544	85.86	6560.98
250	88.5	0.9206	0.6838	86.24	8092.35
300	105.25	1.0915	0.8158	86.78	9558.90
350	122	1.2527	0.9429	87.40	10939.84
400	141	1.4294	1.0737	87.22	12445.36

UNIVERSITY OF ILLINOIS

RECENT AERONAUTICAL AND ASTRONAUTICAL
ENGINEERING DEPARTMENT TECHNICAL REPORTS

Technical Report Number	Title	Author	Journal Publication
AAE 62-1	An Introduction to Viscoelastic Analysis	H. H. Hilton	Engineering Design for Plastics, Reinhold Publ. Corp., N.Y., 199-276 (1964).
AAE 62-2	A Method of Characteristics Analysis of Detonation Stability	R. A. Strehlow	
AAE 63-1	On Non-Stationary White Noise	Y. K. Lin	J. Acoust. Soc. Amer. 36:82-84 (1964).
AAE 63-2	Formulation and Evaluation of Approximate Analogies for Transient Temperature Dependent Linear Viscoelastic Media	H. H. Hilton and J. R. Clements	Proc. Conf. on Thermal Loading and Creep, Inst. Mech. Eng., London, 6.17-6.24(1964).
AAE 63-3	Free Vibrations of Continuous Skin-Stringer Panels with Non-Uniform Stringer Spacing and Panel Thickness	Y. K. Lin, T. J. McDaniel, B. K. Donaldson, C. F. Vail and W. J. Dwyer	AFML-TR-64-347, Wright-Patterson AFB (1965).
AAE 64-1	Random Vibrations of a Myklestad Beam	Y. K. Lin	AIAA J., 2:1448-1451 (1964).
AAE 64-2	On Detonation Initiation	R. A. Strehlow	AIAA J., 2:783-784 (1964).
AAE 64-3	A Theoretical Investigation of a Restrictive Model for Detonation Initiation	R. B. Gilbert	AIAA J., 4:1777-1783 (1966).

RECENT AERONAUTICAL AND ASTRONAUTICAL ENGINEERING DEPARTMENT TECHNICAL REPORTS (continued)

Technical Report Number	Title	Author	Journal Publication
AAE 64-4	Transfer Matrix Representation of Flexible Airplanes in Gust Response Study	Y. K. Lin	J. of Aircraft, 2:116-121 (1965).
AAE 64-5	Dynamic Characteristics of Continuous Skin-Stringer Panels	Y. K. Lin	Acoustical Fatigue in Aerospace Structures, Syracuse Univ. Press, 163-184 (1965).
AAE 64-6	Experimental Study of the Growth of Transverse Waves in Detonations	R. Liaugminas	See AAE 66-3
AAE 64-7	Nonstationary Excitation and Response in Linear Systems Treated as Sequences of Random Pulses	Y. K. Lin	Journal of the Acoustical Society of America, 38:453-460 (1965).
AAE 65-1	Transverse Waves in Detonations	R. A. Strehlow and F. Dan Fernandes	Combustion and Flame, 9:109-119 (1965).
AAE 65-2	A Summary of Linear Viscoelastic Stress Analysis	H. H. Hilton	Solid Rocket Structural Integrity Abstracts, 2:1-56 (1965).
AAE 65-3	Approximate Correlation Function and Spectral Density of the Random Vibration of an Oscillator with Non-Linear Damping	Y. K. Lin	AFMK-TR-66-62, Wright Patterson AFB (1966).
AAE 65-4	Investigation of the Flow Properties Downstream of a Shock Wave Propagating into a Convergent Duct	R. E. Cusey	See AAE 65-6

RECENT AERONAUTICAL AND ASTRONAUTICAL ENGINEERING DEPARTMENT TECHNICAL REPORTS (continued)

Technical Report Number	Title	Author	Journal Publication
AAE 65-5	A Method for the Determination of the Matrix of Impulse Response Functions with Special Reference to Applications in Random Vibration Problems	Y. K. Lin	AFFDL-TR-66-80, Wright Patterson AFB, 743-751 (1966).
AAE 65-6	Convergent Channel Shock Tube for Detonation Initiation Studies	A. J. Crooker	"Detonation and Initiation Behind an Accelerating Shock Wave" by R. A. Strehlow, A. J. Crooker, R. E. Cusey, Comb and Flame, 11:339-351 (1967).
AAE 66-1	A Comparison of Experimental and Theoretical Transverse Wave Spacings in Detonation	R. H. Watson	See AAE 66-3
AAE 66-2	A Simple Model for the Mechanism of Detonation	J. R. Eyman	See AAE 66-3
AAE 66-3	Transverse Wave Structure in Detonations	R. A. Strehlow, R. Liaugminas, R. H. Watson and J. R. Eyman	11th Symposium (Intertional) on Combustion, Mono Book Corp. Baltimore, Md., (1967).
AAE 66-4	A Real Gas Analysis Using an Acoustic Model for the Transverse Wave Spacing in Detonations	R. E. Maurer	AIAA Journal, 7: 323-328, (1969).
AAE 67-1	Shock Tube Studies in Exothermic Systems	R. A. Strehlow	Phys. Fluids, 12: 96-100, (1969).

RECENT AERONAUTICAL AND ASTRONAUTICAL ENGINEERING DEPARTMENT TECHNICAL REPORTS (continued)

Technical Report Number	Title	Author	Journal Publication
AAE 67-2	Shock Tube Chemistry	R. A. Strehlow	Progress in High Temperature Physics and Chemistry, Pergamon Press, N.Y., 2: 127-176 (1968).
AAE 67-3	Structural Failure Criteria for Solid Propellants Under Multiaxial Stresses	A. R. Zak	J. Spacecraft, 5: 265-269 (1968)
AAE 67-4	Structural Analysis of Realistic Solid Propellant Materials	A. R. Zak	J. Spacecraft, 5: 270-275 (1968).
AAE 67-5	Characteristics of Transverse Waves in Detonations of H_2, C_2H_2, C_2H_4 and CH_4 - Oxygen Mixtures	C. D. Engel	AIAA Journal, 7: 492-496 (1969).
AAE 68-1	A Review of Shock Tube Chemistry	R. A. Strehlow	Progress in High Temperature Physics and Chemistry, Pergamon Press, N.Y., 2: 1-146 (1969).
AAE 68-2	On the Interpretation of Molecular Beam Data	A. Klavins	A. Klavins and L. H. Sentman Rev. Sci. Instr., 41: 1560-1567 (197
AAE 68-3	Detonative Mach Stems	R. A. Strehlow H. O. Barthel	
AAE 68-4	On the Strength of Transverse Waves and Geometrical Detonation Cell Model for Gas Phase Detonations	J. R. Biller	R. A. Strehlow and J. R. Biller Comb. and Flame, 13: 577-582, (1970).
AAE 68-5	The MISTRESS User Manual	H. H. Hilton	
AAE 69-1	The Chemical Shock Tube - Implications of Flow Non-Idealities	R. A. Strehlow R. L. Belford	

RECENT AERONAUTICAL AND ASTRONAUTICAL ENGINEERING DEPARTMENT TECHNICAL REPORTS (continued)

Technical Report Number	Title	Author	Journal Publication
AAE 69-2	Phenomenological Investigation of Low Mode Marginal Planar Detonations	A. J. Crooker	Acta Astronautica, 1:303-315(1974).
AAE 69-3	Multi-Dimensional Detonation Wave Structure	R. A. Strehlow	Astronautica Acta, 15:345-358(1970).
AAE 69-4	An Experimental and Analytical Investigation of a Two-Dimensionally Stiffened Panel	A. R. Zak C. E. French	AFML-TR-68-390, Wright-Patterson AFB,(1969).
AAE 69-5	On the Kinetic Equations for a Dilute, Short Range Gas	T. J. Forster L. H. Sentman	with A.D. Grimm, Proc. Ninth International Symposium on Rarefied Gas Dynamics, A3.1-3.8 (1974).
AAE 69-6	The Sawtooth Column of the Supersonic Electric Arc in Sulfur Hexafluoride	C. E. Bond	AIAA J., 9: 510-512 (1971).
AAE 69-7	Theoretical and Experimental Analysis of Stiffened Panels Under Dynamic Conditions	A. R. Zak R. N. Yurkovich J. H. Schmidt	J. of Aircraft, 3: 149-155 (1971).
AAE 70-1	On the Interaction Between Chemical Kinetics and Gas-Dynamics in the Flow Behind a Cylindrical Detonation Front	S. Rajan	
AAE 70-2	Preliminary Studies on the Engineering Applications of Finite Difference Solutions of the Navier-Stokes Equations	W. F. Van Tassell	
AAE 70-3	Some Aspects of the Surface Boundary Condition in Kinetic Theory	A. Klavins	Proc. of International Symposium on Rarefied Gas Dynamics, Pisa, Italy (1970).

RECENT AERONAUTICAL AND ASTRONAUTICAL ENGINEERING DEPARTMENT TECHNICAL REPORTS (continued)

Technical Report Number	Title	Author	Journal Publication
AAE 70-4	A Study of the Transient Behavior of Fuel Droplets during Combustion: Theoretical Considerations for Aerodynamic Stripping	H. Krier	
AAE 70-5	On the Solid Body Model for an Accelerating Electric Arc	F. Klett	
AAE 71-1 UILU-ENG 71 0501	Detonative Mach Stems	R. A. Strehlow H. O. Barthel	
AAE 71-2 UILU-ENG 71 0502	An Investigation of Transient Phenomena in Detonations	R. J. Stiles	with R. A. Strehlow, A. A. Adamczyk, Astronautica Acta, 17: 509-527 (1972)
AAE 71-3 UILU-ENG 71 0503	On the Role of Tangential Velocity Changes in the Scattering of a Molecular Beam from A Solid Surface	C. C. Chrisman L. H. Sentman	Chemical Physics Letters, 26:407-413(1974).
AAE 72-1 UILU-ENG 72 0501	Unconfined Vapor Cloud Explosions - An Overview	R. A. Strehlow	Fourteenth Symposium on Combustion, 1189-1200 (1973).
AAE 72-2 UILU-ENG 72 0502	Application of Illiac IV Computer to Numerical Solutions of Structural Problems	H. H. Hilton A. R. Zak J. J. Kessler P. C. Rockenbach	
AAE 72-3 UILU-ENG 72 0503	On the Measurement of Energy Release Rates In Vapor Cloud Explosions	R. A. Strehlow L. D. Savage G. M. Vance	Combustion Science and Technology, 6: 307-312 (1972).

RECENT AERONAUTICAL AND ASTRONAUTICAL ENGINEERING DEPARTMENT TECHNICAL REPORTS (continued)

Technical Report Number	Title	Author	Journal Publication
AAE 72-4 UILU-ENG 72 0504	A Performance Comparison of Several Numerical Minimization Algorithms	J. E. Prussing	
AAE 73-1 UILU-ENG 73 0501	Stresses and Damping in the Matrix of a Composite Material	A. R. Zak	
AAE 73-2 UILU-ENG 73 0502	Early Burning Anomalies in the XM 645 Flechette Cartridge	H. Krier D. R. Hall	BRL Rept. No. 104 (1973).
AAE 73-3 UILU-ENG 73 0503	Equivalent Explosive Yield of the Explosion in the Alton Southern Gateway Yard, East St. Louis, Ill., January 22, 1972	R. A. Strehlow	
AAE 73-4 UILU-ENG 73 0504	Failure Studies of Gaseous Detonations	R. J. Salm	Acta Astronautica (in press).
AAE 73-5 UILU-ENG 73 0505	An Investigation of Hydrogen-Oxygen-Argon Detonations	J. R. Biller	
AAE 73-6 UILU-ENG 73 0506	Interior Ballistic Predictions Using Data From Closed and Variable-Volume Simulators	H. Krier S. A. Shimpi M. J. Adams	Proc. 11th JANNAF Combustion Meeting, CPIA Publ. 261:17-30(1974).
AAE 73-7 UILU-ENG 73 0507	Theory of Rotationally Symmetric Laminar Premixed Flames	G. M. Vance H. Krier	Comb. and Flame J., 22: 365-375 (1974).
AAE 73-8 UILU-ENG 73 0508	Burning of Fuel Droplets at Elevated Pressures	J. H. Rush H. Krier	Comb. and Flame J., 22: 377-382 (1974).
AAE 73-9 UILU-ENG 73 0509	An Impact Ignition Model for Solid Propellants	H. Krier H. H. Hilton O. Olorunsola D. L. Reuss	BRL Rept. No. 1707 (1974).

RECENT AERONAUTICAL AND ASTRONAUTICAL ENGINEERING DEPARTMENT TECHNICAL REPORTS (continued)

Technical Report Number	Title	Author	Journal Publication
AAE 73-10 UILU-ENG 73 0510	Optimal Multiple-Impulse Direct Ascent Fixed-Time Rendezvous	J. E. Prussing L. R. Gross	AIAA J., 12, 885-889 (1974).
AAE 73-11 UILU-ENG 73 0511	The Structure and Stability of Detonation Waves	R. A. Strehlow	
AAE 74-1 UILU-ENG 74 0501	Model of Flame Spreading and Combustion Through Packed Beds of Propellant Grains	H. Krier W. F. Van Tassell S. Rajan J. T. Ver Shaw	BRL Report No. 147 (1974). Int. J. Heat-Mass Transfer, 1377-86 (1975).
AAE 74-2 UILU-ENG 74 0502	On the Nature of Non-Ideal Blast Waves	R. A. Strehlow A. A. Adamczyk	WSS/CI Paper No. 74-12, Pullman, Wash. (1974).
AAE 74-3 UILU-ENG 74 0503	Viscous Incompressible Flow in Spiral Channels	W. F. VanTassell	
AAE 74-4 UILU-ENG 74 0504	Frequency Response Functions of a Disordered Periodic Beam	J. N. Yang Y. K. Lin	J. Sound and Vibration 38: 317-340 (1975).
AAE 74-5 UILU-ENG 74 0505	Predicting Uniform Gun Interior Ballistics: Part I. An Analysis of Closed Bomb Testing	H. Krier S. A. Shimpi	Comb. and Flame J. 25: 229-240 (1975).
AAE 74-6 UILU-ENG 74 0506	Predicting Uniform Gun Interior Ballistics: Part II. The Interior Ballistic Code	H. Krier M. J. Adams	Proc. 11th JANNAF Comb. Meeting, CPIA Publ. 261: 17-30 (1974).
AAE 74-7 UILU-ENG 74 0507	Predicting Uniform Gun Interior Ballistics: Part III. The Concept and Design of the Dynagun Ballistic Simulator	H. Krier J. W. Black	Proc. 11th JANNAF Comb. Meeting, CPIA Publ. 261: 31-43(1974).
AAE 74-8 UILU-ENG 74 0508	Process of Fluidization During Porous Solid Propellant Combustion	H. Krier J. T. Ver Shaw	AIAA Paper 75-242 (1975).
AAE 74-9 UILU-ENG 74 0509	An Analysis of Flame Propagation Through Coal Dust-Air Mixtures	J. L. Krazinski H. Krier	AIAA Paper 74-1111 (1974).

RECENT AERONAUTICAL AND ASTRONAUTICAL ENGINEERING DEPARTMENT TECHNICAL REPORTS (continued)

Technical Report Number	Title	Author	Journal Publication
AAE 74-10 UILU-ENG 74 0510	An Interior Ballistics Prediction of the M549 Rocket Assisted Projectile	H. Krier S. Shimpi E. Meister	
AAE 75-1 UILU-ENG 75 0501	Dynamically Induced Thermal Stresses in Composite Material, Structural Panels	A. Zak W. Drysdale	
AAE 75-2 UILU-ENG 75 0502	Numerical Analysis of Laminated, Orthotropic Composite Structures	A. R. Zak	
AAE 75-3- UILU-ENG 75 0503	The Characterization and Evaluation of Accidental Explosions	R. A. Strehlow W. E. Baker	*NASA CR 134779* (June 1975). Also Progr. Energy & Comb. Sc. (in press).
AAE 75-4 UILU-ENG 75 0504	Program Manual for the Eppler Airfoil Inversion Program	W. G. Thomson	
AAE 75-5 UILU-ENG 75 0505	Design of High Lift Airfoils with a Stratford Distribution by the Eppler Method	W. G. Thomson	
AAE 75-6 UILU-ENG 75 0506	Prediction of Flame Spreading and Pressure Wave Propagation in Propellant Beds	H. Krier	AIAA J. 14: 301-309 (1976)
AAE 75-7 UILU-ENG 75 0507	Vigorous Ignition of Granulated Beds by Blast Impact	H. Krier S. Gokhale	Int. J. Heat-Mass Transfer 19: 915-923 (1976)
AAE 75-8 UILU-ENG 75 0508	Solid Propellant Burning Evaluation with the Dynagun Ballistic Simulator	H. Krier T. G. Nietzke M. J. Adams J. W. Black E. E. Meister	J. Ballistics 1: 103-149 (1976)
AAE 75-9 UILU-ENG 75 0509	Structural Reliability & Minimum Weight Analysis for Combined Random Loads & Strengths	H. H. Hilton	AIAA J. (in press)

RECENT AERONAUTICAL AND ASTRONAUTICAL ENGINEERING DEPARTMENT TECHNICAL REPORTS (Continued)

Technical Report Number	Title	Author	Journal Publication
AAE 75-10 UILU-ENG 75 0510	Linear Viscoelastic Analysis with Random Material Properties	H. H. Hilton J. Hsu J. S. Kirby	
AAE 76-1 UILU-ENG 76 0501	Two Degree of Freedom Flutter of Linear Viscoelastic Wings in Two Dimensional Flow	C. F. Vail H. H. Hilton	In press AIAA J.
AAE 76-2 UILU-ENG 76 0502	An Error Analysis of Computerized Aircraft Synthesis	V. V. Volodin H. H. Hilton	In press J. of Aircraft
AAE 76-3 UILU-ENG 76 0503	Reactive Two-Phase Flow Models Applied to the Prediction of Detonation Transition in Granulated Propellant	H. Krier M. Dimitstein S. S. Gokhale	AIAA J. 16: 177-183 (1978)
AAE 76-4 UILU-ENG 76 0504	Transient Temperature Response of Charring Composite Slabs	J. E. Prussing H. Krier	Int'l J. Heat Mass Transfer. 21: 519-522 (1978)
AAE 76-5 UILU-ENG 76 0505	Nonlinear Response of Laminated Composite Material Cylindrical Shells	A. R. Zak J. N. Craddock	
AAE 76-6 UILU-ENG 76 0506	An Investigation of Blast Waves Generated from Non-Ideal Energy Sources	A. A. Adamczyk	
AAE 77-1 UILU-ENG 77 0501	Nonlinear Dynamic Analysis of Flat Laminated Plates by the Finite Element Method	A. R. Zak	
AAE 77-2 UILU-ENG 77 0502	An Investigation of Blast Waves Generated by Constant Velocity Flames	R. T. Luckritz	
AAE 77-3 UILU-ENG 77 0503	On the Blast Waves Produced by Constant Velocity Combustion Waves	R. A. Strehlow R. D. Luckritz	
AAE 77-4 UILU-ENG 77 0504	Direct Initiation of Detonation by Non-Ideal Blast Waves	R. J. Cesarone	
AAE 77-5 UILU-ENG 77 0505	The Blast Wave Generated by Constant Velocity Flames	S. A. Shimpi R. A. Strehlow	

RECENT AERONAUTICAL AND ASTRONAUTICAL ENGINEERING DEPARTMENT TECHNICAL REPORTS (Continued)

Technical Report Number	Title	Author	Journal Publication
AAE 77-6 UILU-ENG 77 0506	Exploratory Studies of Flame and Explosion Quenching	R. A. Strehlow L. C. Sorenson L. D. Savage H. Krier	
AAE 77-7 UILU-ENG 77 0507	The Trajectory of a Liquid Droplet Injected Into the Wake of an Aircraft in Ground Effect	M. B. Bragg	
AAE 77-8 UILU-ENG 77 0508	Comparison of Viscoelastic and Structural Damping in Flutter	H. H. Hilton	
AAE 77-9 UILU-ENG 77 0509	The Blast Wave Generated by Constant Velocity Flames	R. A. Strehlow R. T. Luckritz A. A. Adamczyk S. Shimpi	
AAE 77-10 UILU-ENG 77 0510	Wind Energy: History, Economics, and the Vertical Wind Turbine	T. R. Richards	
AAE 77-11 UILU-ENG 77 0511	Final Report: Low Speed Airfoil Study	A. I. Ormsbee	
AAE 77-12 UILU-ENG 77 0512	Final Report: Propeller Study, Part I, Introduction and Overview	A. I. Ormsbee	
AAE 77-13 UILU-ENG 77 0513	Final Report: Propeller Study, Part II, The Design of Propellers for Minimum Noise	C. J. Woan	
AAE 77-14 UILU-ENG 77 0514	Final Report: Propeller Study, Part III, Experimental Determination of Thrust & Torque on the YO-3A Aircraft	S. A. Siddiqi K. R. Sivier A. I. Ormsbee	
AAE 77-15 UILU-ENG 77 0515	Direct Initiation of Detonation	R. A. Strehlow H. O. Barthel	

RECENT AERONAUTICAL AND ASTRONAUTICAL ENGINEERING DEPARTMENT TECHNICAL REPORTS (Continued)

Technical Report Number	Title	Author	Journal Publication
AAE 77-16 UILU-ENG 77 0516	The Effects of Energy Distribution Rates and Density Distribution on Blast Wave Structure	R. A. Strehlow L. H. Sentman	
AAE 77-17 UILU ENG 77 0517	Modeling of Convective Mode Combustion Through Granulated Propellant to Predict Transition to Detonation	H. Krier J. A. Kezerle	17th Combustion Symposium: In Press
AAE 78-1 UILU ENG 78 0501	Unsteady Internal Boundary Layer Flows with Application to Gun Barrel Heat Transfer and Erosion	M. J. Adams H. Krier	
AAE 78-2 UILU ENG 78 0502	Extracting Burning Rates for Multiperforated Propellant from Closed Bomb Testing	H. Krier	
AAE 78-3 UILU ENG 78 0503	Lean Limit Flammability Study of Methane-Air Mixtures in a Square Flammability Tube	J. Jarosinski R. A. Strehlow	
AAE 78-4 UILU ENG 78 0504	Interim Technical Report AFOSR 77-3336: "An Investigation of the Ignition Delay Times For Propylene Oxide-Oxygen-Nitrogen Mixtures"	E. E. Meister	
AAE 78-5 UILU ENG 78 0505	Final Report: A Distribution Model for the Aerial Application of Granular Agricultural Particles	S. T. Fernandes A. I. Ormsbee	
AAE 78-6 UILU ENG 78 0506	The Thermal Structure of a Methane-Air Flame Propagating in a Square Flammability Tube	J. Jarosinski R. A. Strehlow	
AAE 78-7 UILU ENG 78 0507	The Effects of Energy Distribution Rates and Density Distribution on Blast Wave Structure	R. A. Strehlow L. H. Sentman	
AAE 78-8 UILU ENG 78 0508	The Effect of a Zero G Environment on Flammability Limits as Determined Using a Standard Flammability Tube Apparatus	R. A. Strehlow D. L. Reuss	

RECENT AERONAUTICAL AND ASTRONAUTICAL ENGINEERING DEPARTMENT TECHNICAL REPORTS (Continued)

Technical Report Number	Title	Author	Journal Publication
AAE 79-1 UILU-ENG 79 0501	An Approximate Finite Element Method of Stress Analysis of Non-Axisymmetric Bodies with Elastic-Plastic Material	J. N. Craddock A. R. Zak	
AAE 79-2 UILU-ENG 79 0502	Stability of Bridge Motion in Turbulent Winds	Y. K. Lin S. T. Ariaratnam	
AAE 79-3 UILU ENG 79 0503	Rotor Blade Dynamics in Hovering Flights	C.Y.R. Hong	
AAE 79-4 UILU ENG 79 0504	Finite Element Analysis of A Dynamically Loaded Flat Laminated Plate	D. W. Pillasch A. R. Zak	
AAE 79-5 UILU ENG 79 0505	An Efficient Rotational Nonequilibrium Model of a CW Chemical Laser	L. H. Sentman	
AAE 79-6 UILU ENG 79 0506	Column Response to Vertical-Horizontal Earthquakes	Y. K. Lin T. Y. Shih	
AAE 79-7 UILU ENG 79 0507	Users Guide for Programs MNORO & AFOPTMNORO	L. H. Sentman	
AAE 79-8 UILU ENG 79 0508	The Blast Wave from Deflagrative Explosions, an Acoustic Approach	R. A. Strehlow	
AAE 80-1 UILU ENG 80 0501	Gas Flow Resistance Measurements Through Packed Beds at High Reynolds Numbers	S. F. Wilcox H. Krier	
AAE 80-2 UILU ENG 80 0502	Fluid Mechanical Processes of Deflagration to Detonation Transition in Beds of Porous Reactive Solids	S. Hoffman H. Krier	
AAE 80-3 UILU ENG 80 0503	Dynamic Analysis of Orthotropic, Layered Plates Subject to Explosive Loading	D. W. Pillasch A. R. Zak	